AD-A096 154 JAYCOR ALEXANDRIA VA F/G 20/7
A REPORT ON COLLECTIVE ION ACCELERATION VIA SPACE CHARGE WAVES --ETC(U
FEB 81 F MAKO, R LUCEY N00173-80-C-0039
UNCLASSIFIED JAYCOR-PSD-200-81-002-FR NL

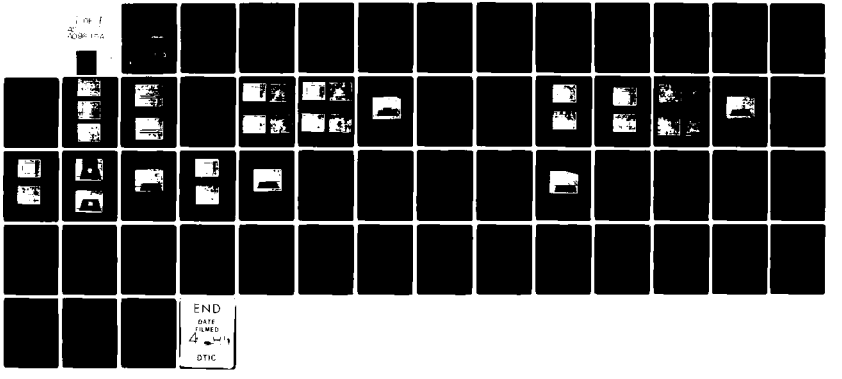

END
DATE FILMED
4-81
DTIC

LEVEL II

12

B.S.

AD A096154

JAYCOR

DTIC
ELECTE
MAR 1 0 1981
S D
F

DDC FILE COPY

81 2 18 238

205 South Whiting Street
Alexandria, Virginia 22304

A REPORT ON COLLECTIVE ION ACCELERATION VIA SPACE CHARGE WAVES ON INTENSE RELATIVISTIC ELECTRON BEAMS

JAYCOR Project 6187

JAYCOR Final Report No. PSD-200-81-002-FR
Contract No. N00173-80-C-0039

February 1981

Frederick Mako and Robert Lucey

JAYCOR
205 S. Whiting Street
Alexandria, VA 22304

Submitted to:

Naval Research Laboratory
Washington, DC 20375

Unclassified

SECURITY CLASSIFICATION OF THIS PAGE (When Data Entered)

REPORT DOCUMENTATION PAGE

READ INSTRUCTIONS BEFORE COMPLETING FORM

1. REPORT NUMBER: PSD-200-81-002-FR
2. GOVT ACCESSION NO.: AD-A096154
3. RECIPIENT'S CATALOG NUMBER:

4. TITLE (and Subtitle): A REPORT ON COLLECTIVE ION ACCELERATION VIA SPACE CHARGE WAVES ON INTENSE RELATIVISTIC ELECTRON BEAMS
5. TYPE OF REPORT & PERIOD COVERED: Final Report 12/20/79 to 12/19/80
6. PERFORMING ORG. REPORT NUMBER: PSD-200-81-002-FR

7. AUTHOR(s): Frederick Mako [redacted] Robert Lucey
8. CONTRACT OR GRANT NUMBER(s): N00173-80-C-0039

9. PERFORMING ORGANIZATION NAME AND ADDRESS:
JAYCOR
205 South Whiting Street
Alexandria, VA 22304

10. PROGRAM ELEMENT, PROJECT, TASK AREA & WORK UNIT NUMBERS: 61153N

11. CONTROLLING OFFICE NAME AND ADDRESS:
Naval Research Laboratory
Washington, DC 20375

12. REPORT DATE: February 1981
13. NUMBER OF PAGES: 56

14. MONITORING AGENCY NAME & ADDRESS (if different from Controlling Office): Same as block 11

15. SECURITY CLASS. (of this report): unclassified
15a. DECLASSIFICATION/DOWNGRADING SCHEDULE:

16. DISTRIBUTION STATEMENT (of this Report)

DISTRIBUTION STATEMENT A
Approved for public release;
Distribution Unlimited

17. DISTRIBUTION STATEMENT (of the abstract entered in Block 20, if different from Report)

Final rpt. 20 Dec 79 – 19 Dec 80

18. SUPPLEMENTARY NOTES

19. KEY WORDS (Continue on reverse side if necessary and identify by block number)

20. ABSTRACT (Continue on reverse side if necessary and identify by block number)

DD FORM 1 JAN 73 1473 EDITION OF 1 NOV 65 IS OBSOLETE
S/N 0102-LF-014-6601

unclassified 392 153
SECURITY CLASSIFICATION OF THIS PAGE (When Data Entered)

CONTENTS

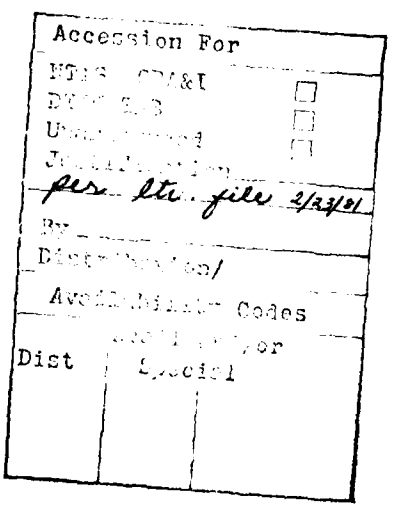

I. INTRODUCTION

Collective methods of ion acceleration using intense relativistic electron beams (IREB) have stimulated a great deal of interest in the past few years.[1,2] The main virtue of an IREB collective ion accelerator is the high internal electric field strength. The primary drawback has been an insufficient ion energy gain or inadequate scaleability.

The interesting property of an intense relativistic electron beam that is useful for collective ion acceleration, .s the large self-electric field. Electric field strengths of 1MV/cm are realizable within the electron beam. By comparison, conventional accelerators, are capable of about 1/100 of this electric field strength. Such a weak electric field in these accelerators results from technical difficulties (e.g insulator breakdown) in trying to produce a vacuum supported electric field. However, conventional accelerators have been shown to be scaleable. That is, ion energy can be increased by either passing the particle many times through a stationary electric field or by being continually accelerated by a moving electric field, up to a theoretical limit. Collective ion accelerators have attempted to utilize the moving electric field approach and have shown limited scaleability.

If collective ion accelerators were scaleable over about 10 meters, at electric field strengths of 1MV/cm, then the result would be a compact, efficient ion accelerator which is capable of producing high energy and high current ion beams. With the currently available electron beam technology, ion beams of a few ten's of kA and a few hundred Mev per nucleon are possible. A collective ion accelerator in the above parameter regime could find an application in areas such as directed energy research, and inertial and magnetic confinement fusion.

One approach that appears to be promising in terms of scaleability is the Converging Guide Collective Ion Accelerator (CGA).[3] In the CGA, ions are trapped and accelerated in negative energy-space charge waves. The space charge waves are grown on and travel with a propagating non-neutral IREB. The wave phase velocity in a conducting cylinder depends on the ratio of beam to wall ratio, where the phase velocity increases inversely with the radii ratio. Thus, wave acceleration is accomplished by passing the electron beam through a grounded metal drift tube that has a decreasing radius in the direction of propagation. The electron beam and hence ions are radially confined by a strong axial magnetic field. Aside from scaleability the CGA also has the advantage of being able to produce a long pulse of ions as compared to the Beam Front type of Collective Ion Accelerator.[4]

The CGA scheme also has several difficulties. One of the primary problems of the CGA is that it is technically very difficult to obtain low phase velocity waves.[5] Low phase velocities are important, since compact intense ion sources do not exist with ion velocities greater than about two-tenths of the speed of light. The wave phase velocity turns out to be very sensitive to variations in the diode current and voltage.

It became necessary during the contractual period to add to the proposed program. One addition was prompted by the physics of the problem. That is, the physics of the space charge wave acceleration program put very stringent conditions on the required beam quality. Thus it became necessary to produce a very flat (~1%) diode current and voltage pulse, i.e., a high quality beam. An extensive study for generating a high quality electron beam has been done and is presented in Section II. In Section III an intense ion injector study was conducted by the method of computer simulation. The last addition to the proposal was a design for producing a toroidal magnetic

field. This field will be needed in a future study of high energy and high current electron beams.

FIGURE CAPTIONS

Fig. 1 Experimental apparatus.

Fig. 2 Reduction of diode current ripple by increasing the inductance before the diode. Short circuit load.

Fig. 3 Photographs of the inductors used to reduce current ripple (Fig. 2).

Fig. 4 Reduction of ripple in the diode voltage and current and the anode current. Beam load without a magnetic field.

Fig. 5 Reduction of ripple in the diode voltage and current and the anode current. Beam load with a 3.5 kG magnetic field.

Fig. 6 Photograph of the inductor form used to reduce ripple (in Figs. 4 and 5).

Fig. 7 Demonstration that skin resistance is not responsible for ripple removal.

Fig. 8 Demonstration that dielectric loss is not responsible for ripple removal.

Fig. 9 Reduction of diode voltage overshoot by using a brush cathode.

Fig. 10 Photograph of brush cathode used to produce the results in Fig. 9.

Fig. 11 Re-occurrence of overshoot during beam propagation study.

Fig. 12 Photographs of the graphite anode used in the beam propagation study.

Fig. 13 Photograph of the cathode stock and cathode tip used to produce the results in Figure 11.

Fig. 14 Removal of overshoot during beam propagation using a graphite brush cathode.

Fig. 15 Photograph of brush cathode used to remove overshoot (Fig. 14).

Fig. 16 Transmitted beam current versus diode impedance at different magnetic field strengths, using axial brush cathode.

Fig. 17 Transmitted beam current versus diode impedance at different magnetic field strengths using a long radial brush cathode.

Fig. 18 Photograph of the long radial brush cathode used to produce the results in Fig. 17.

Fig. 19 Racetrack induction accelerator

Fig. 20 Toroidal magnetic field

Fig. 21 The G factor of (1.23) $G(\alpha, \beta)$, for a uniform current density coil. Contours of constant $G(\alpha, \beta)$ are plotted versus the normalized geometry of the coil α and β.

Fig. 22 The attentuation factor, $k(d)$, which determines the magnitude of the peak current in a damped discharge.

Fig. 23 Roughess parameters for pipes and tubes.

Fig. 24 The fanning friction factor as a function of Re and D/e.

II. Electron Beam Quality from a Long Pulse Artificial Pulse Line and a Cold Cathode

A) Technical Background

The success of many experiments today can be very dependent on the electron beam quality. Collective Ion Acceleration by Space Charge Waves, Free Electron Lasers and Gyrotrons are a few examples of experiments that depend on beam quality. For the CGA scheme both the wave phase velocity and electric field strength depend on the beam current and electron energy. In a Free Electron Laser the wavelength depends on the inverse square of the electron energy. Both frequency and radiation efficiency are dependent on the electron energy in gyrotrons. A high quality beam is one that is mono-energetic in a given direction at constant current over the desired pulse length. This report addresses just the issues of producing a mono-energetic, constant current beam.

In each of the above listed experiments, a high voltage ($\geq$100 KV) long pulse ($\geq$300 ns) beam is very desireable. The long pulse length excludes transmission line technology. Thus, one is left with lumped parameter (artificial) pulse lines and pulse transformers. Both of the above technologies requires compensation techniques to achieve a constant voltage and current. Pulse transformers have the inherent problem of a frequency dependent impedance Artificial pulse lines have a ripple due to discrete elements. And when an artificial line is used in conjunction with a cold cathode diode for long pulses, another difficulty occurs. In order to reduce voltage droop, due to diode closure, a large diode gap is required. With a large gap the emission electric field is reduced, thus diode "turn on" becomes difficult and an overshoot occurs in the diode voltage. Techniques are developed below for eliminating substantial amounts of the above problems.

B) Experimental Apparatus

Figure 1 is a side view of the experimental system. High voltage is formed by series stacking artificial pulse lines. The output parameters into a matched load are 450 KV, 1.5 KA for 300 ns FWHM. The high voltage is insulated from the surrounding ground plane by liquid freon. Primarily two types of diode insulators were used. A simple flat radial insulator was initially used but had breakdown problems. Later an axially capacitive graded ring insulator was found to work satisfactorily (depicted in Fig. 1). Several diode geometries were tried. These are discussed in the text. Figure 1 shows a foilless diode arrangement that was used during the beam propagation experiments.

C) Results

Voltage and Current Ripple from an Artificial Pulse Line

Figure 2 shows the effect on the diode current as the inductance of the "integrating coil" is increased between the high voltage lines (Fig. 1) and the diode. In Fig. 2A a 1" diameter aluminum shaft that is 19" long makes the connection between the high voltage stack and the diode. Figure 2B is the diode current when a 6.5 μH coil is used. Figure 3A is a photograph of the inductor that was used to produce the diode current trace in Fig. 2B. The inductor in Fig. 3A is constructed by winding 2 mm diameter tinned copper wire on a grooved 1" diameter nylon rod. The nylon rod was 19" long and 4 turns of wire per inch was wound over 17"'s of the rod length. Figure 2C is the diode current when a 27μH coil is used. Figure 3B is a photograph of the inductor that was used to produce the diode current trace in Fig. 2C. The inductor in Figure 3B is constructed by winding 1 mm diameter tinned copper wire on a grooved 1" diameter nylon rod.

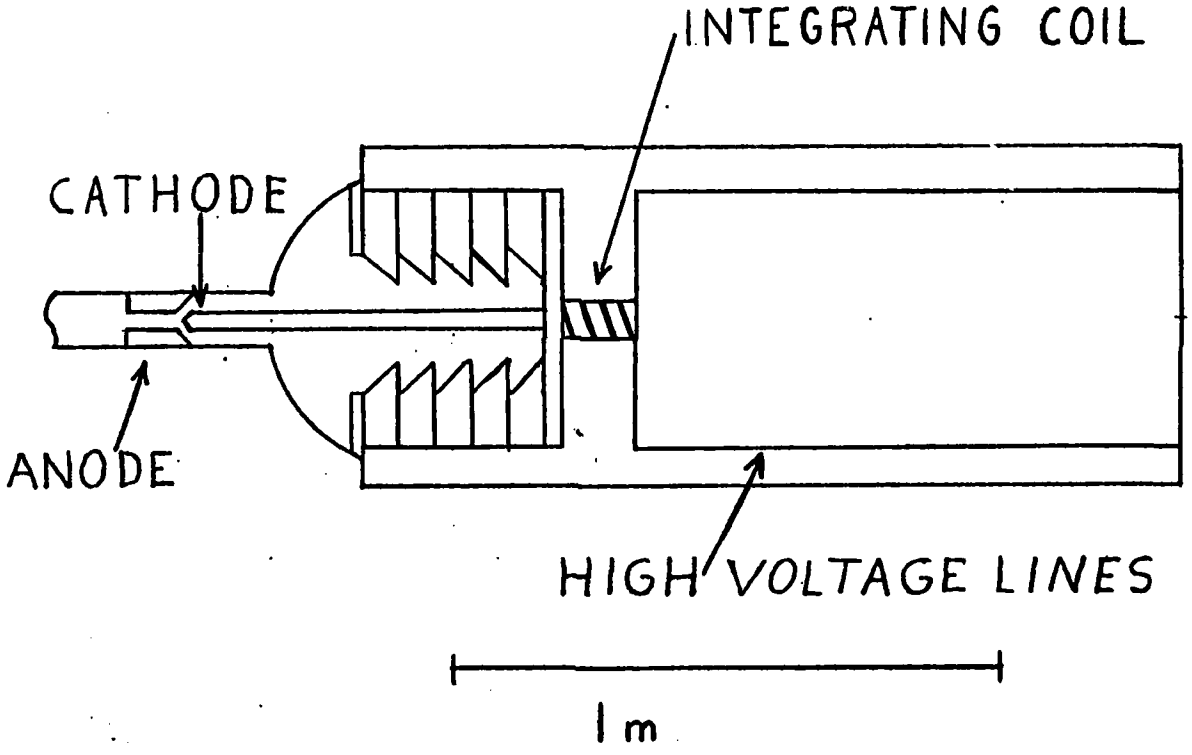

Figure 1

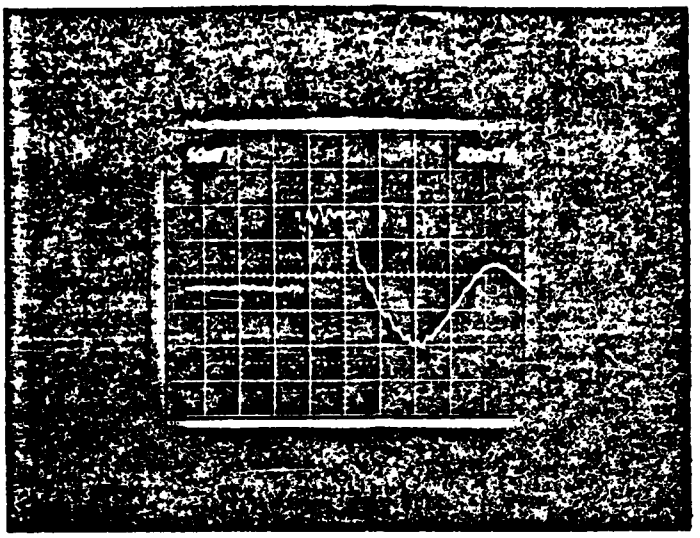

A

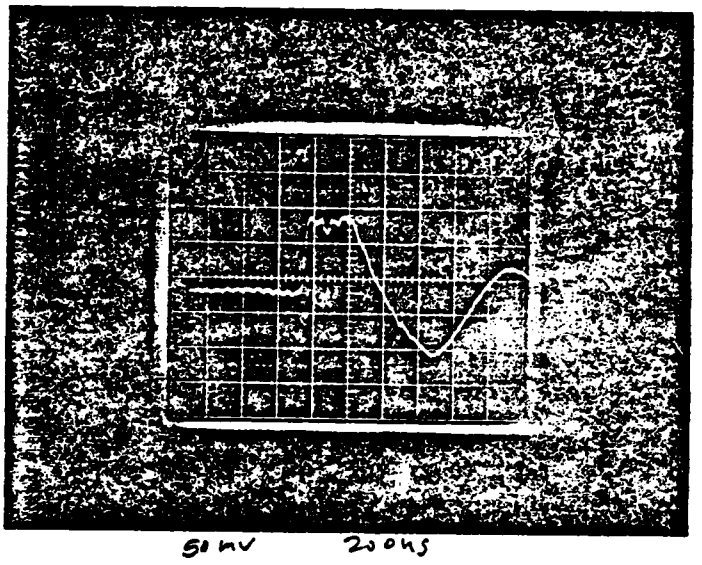

B

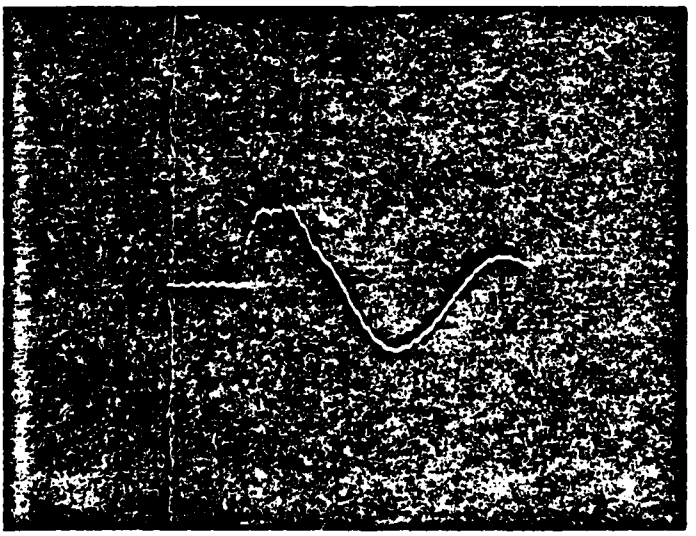

C

Figure 2

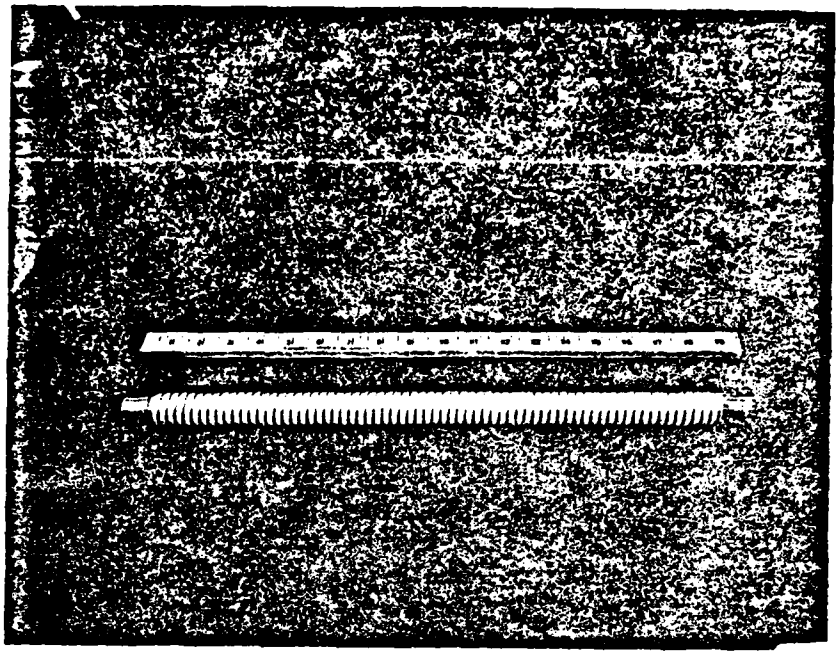

A

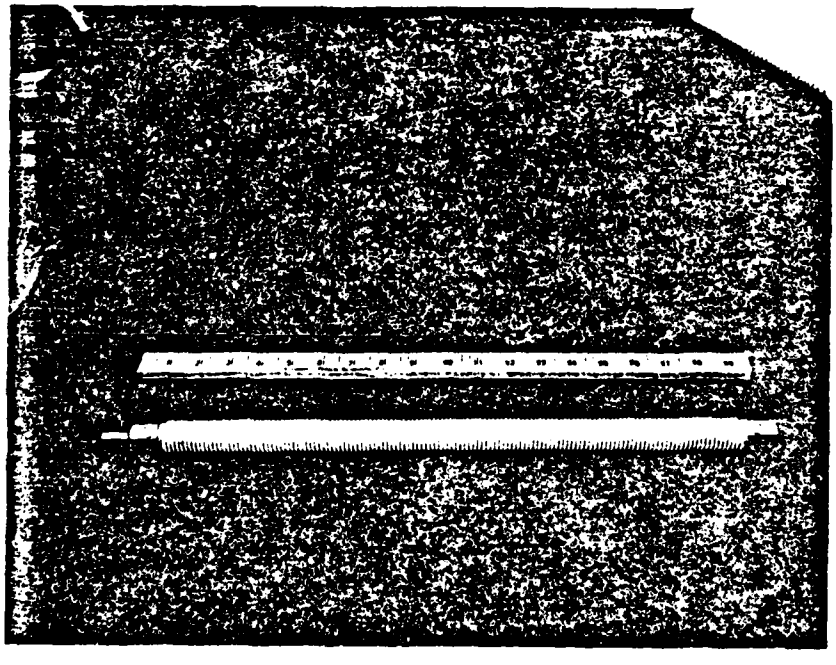

B

Figure 3

The nylon rod was 19" long and 8 turns of wire per inch was wound over 17"'s of the rod length. As can be observed from Figures 2A, B, C, a reduction of the current ripple is accomplished.

The idea behind the coil is that for very high frequencies the coil behaves like a high impedance transmission line. Thus for high frequencies, the signal is reflected back and forth between the high voltage line and inductor until it is dissipated. The coil in Figure 3B has an impedance of about 1kΩ for pulses with rise times less than the transmit time of 26 nsec. For frequencies with rise times greater than 26 n sec the inductor no longer behaves like a pulse line but as a lumped parameter, namely, as an inductor. But the L/R time of the coil is short (≈38 nsec) and thus has little affect on low frequencies.

The load used in Figure 2A, B, C was a short circuit provided by a poor insulator design. It is important to know how this ripple removing method behaves when an electron beam load is used, with and without an external magnetic field. Thus the previous diode insulator was changed to one that would support the diode voltage for the full pulse length. The results of a beam load are shown in Figures 4 and 5.

In Figure 4, A and B are without an integrating coil (inductor) in the beam generator while Figures 4 C and D are with a 20 μH coil (Fig. 6). In A the top trace is the diode voltage and the bottom is the Faraday Cup current. The top trace in B is the diode current. Figure C can be directly compared with A. In D the signal sensitivity was doubled and the signal inverted as compared to B. There was no magnetic field applied. A hemispherical graphite brush cathode (Fig. 10) was used with a 2 cm spacing to a graphite disc anode. The anode also served as the collector for the Faraday Cup.

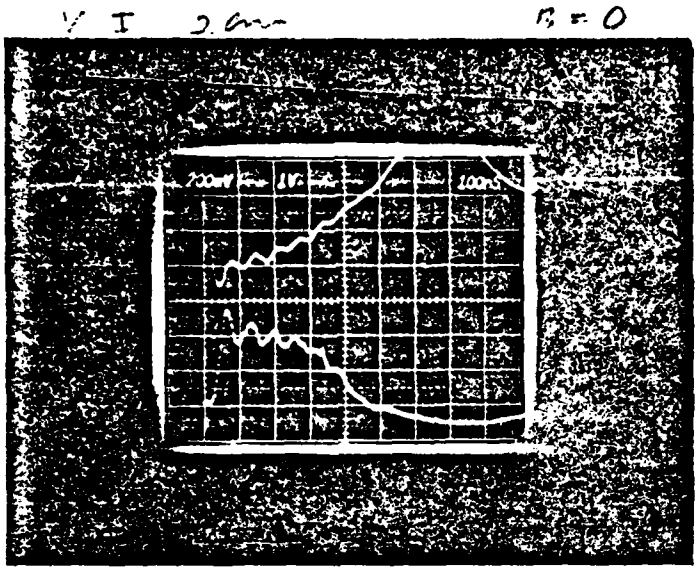

A

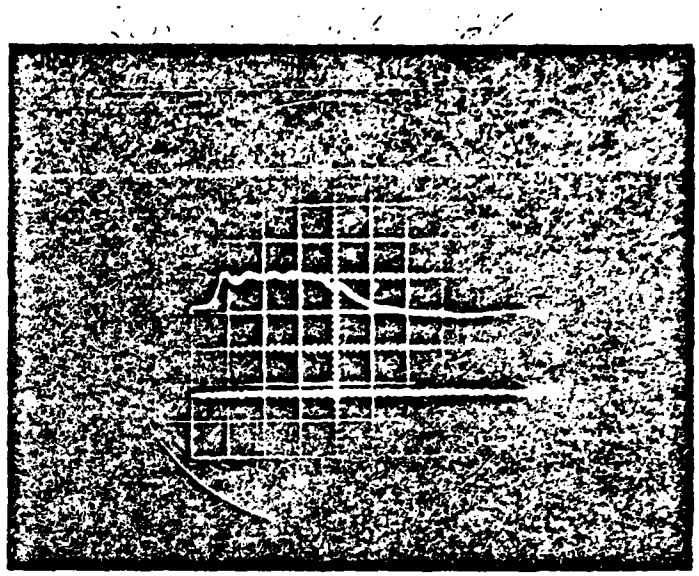

B

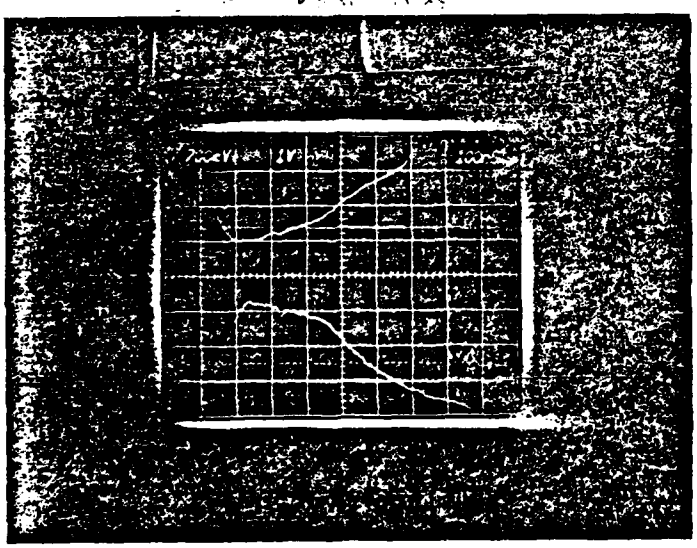

C

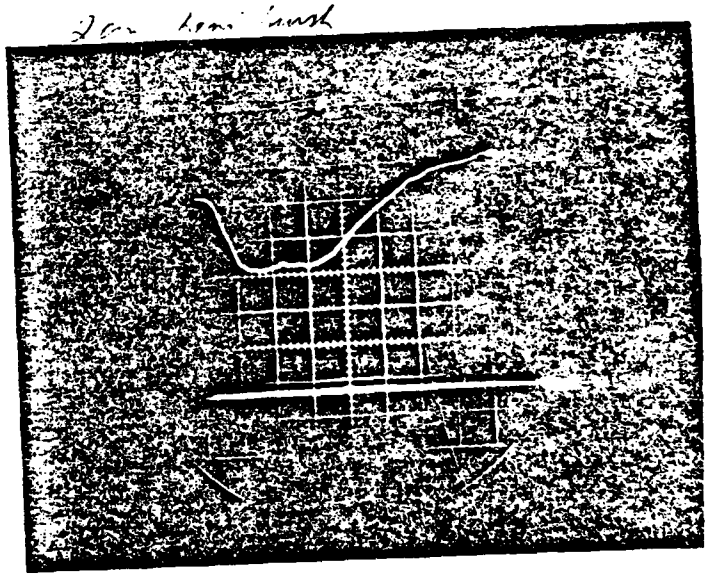

D

Figure 4

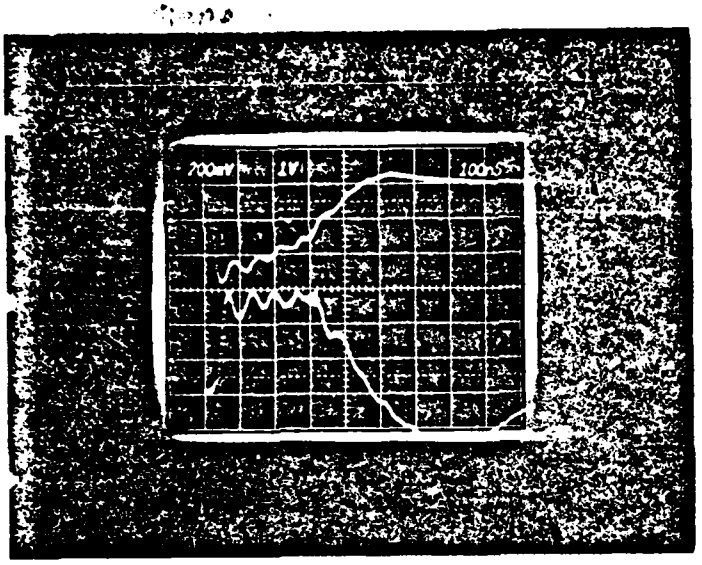

A

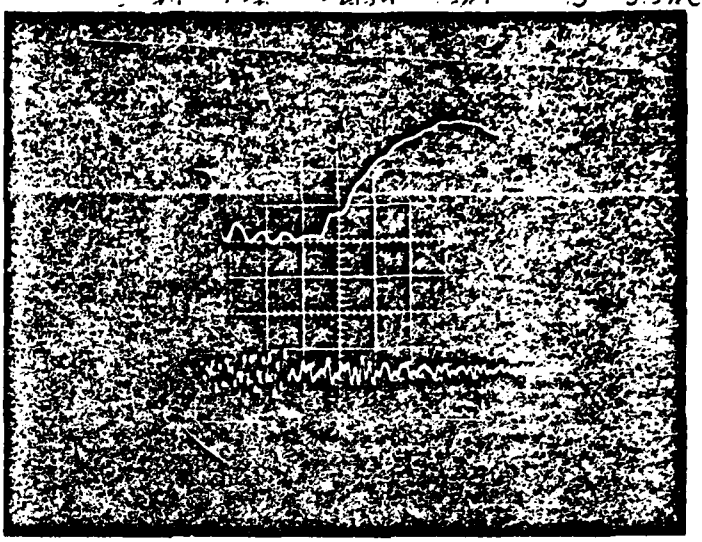

B

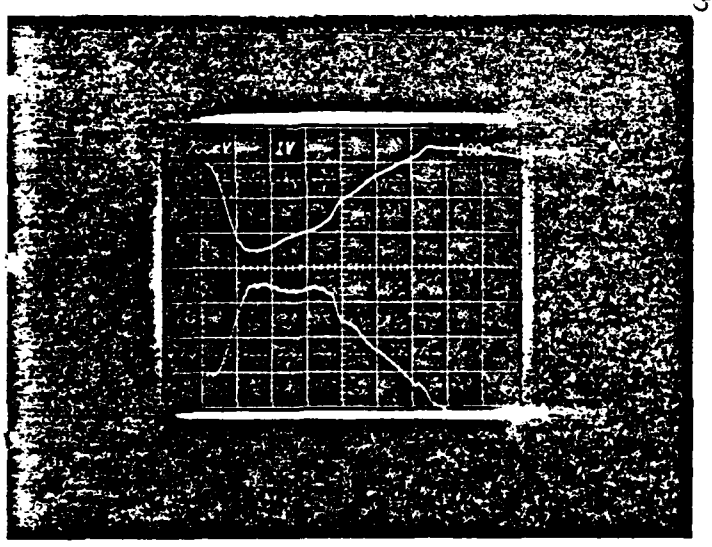

C

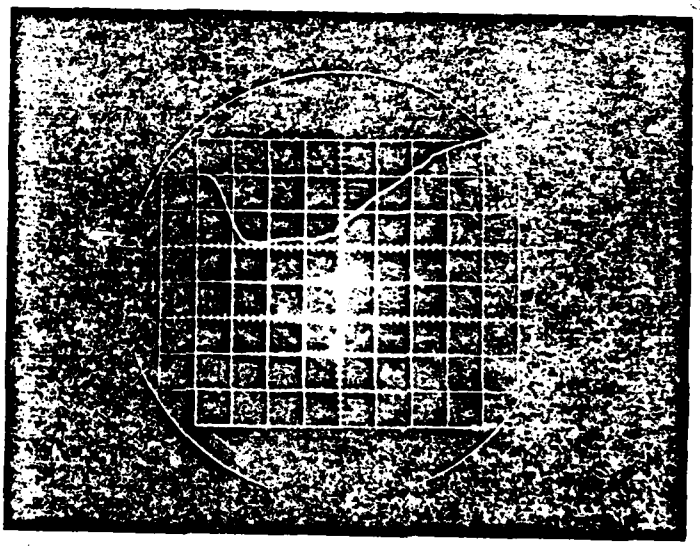

D

Figure 5

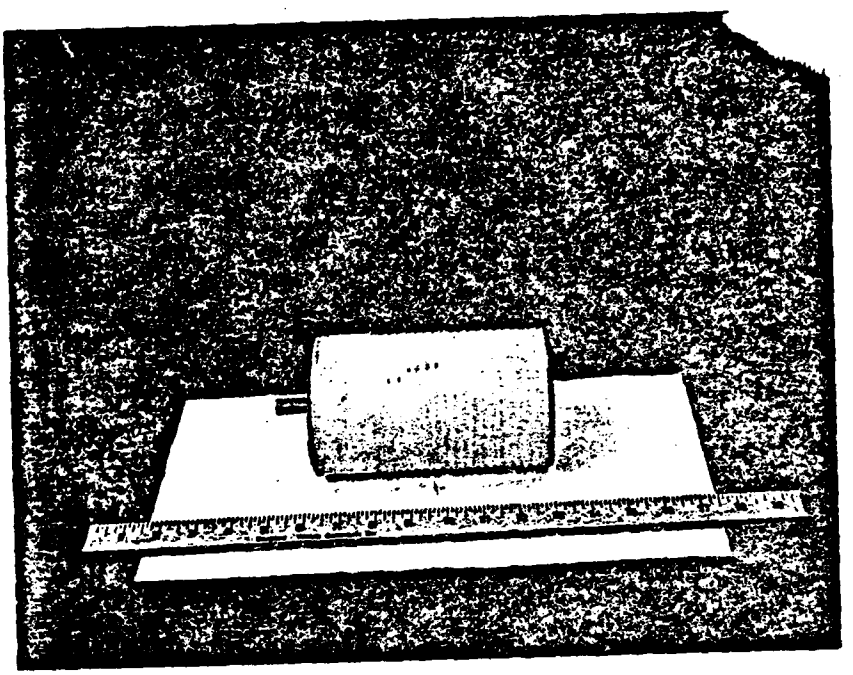

Figure 6

Figures 5A and B are without an inductor in the beam generator. Figure 5C and D are with a 20 μH coil (Fig. 6). In A the top trace is the diode voltage and the bottom is the Faraday Cup current. The top trace in B is the diode current. Figures C and D can be directly compared with A and B, respectively. Now, a 3.5 kG axial magnetic field is applied. All other conditions were the same as in Figures 4A, B, C, D.

Figure 6 is a photograph of the coil form used to produce the results in Figures 4 and 5A, B, C, D. Twenty turns of 1 mm diameter tinned copper wire was wound on a 4" diameter nylon rod over a length of 5". This 20 μH coil formed a line impedance of about 1 kΩ (∿ three times the line impedance) with a one way transit time of 20 nsec.

It is quite clear that the inductor removes the ripple from the beam voltage and current. However, there is still some question about the mechanism by which the parasitic ripple is removed. For example,how large is the skin effect in the tinned copper or how lossy is the nylon form.

In order to show that the ripple removal was not due to the skin effect, a low skin resistance coil was used. The original coil (Fig. 6) had a skin resistance of about 80 ohms at 1GHz. This resistance can be reduced to about 9Ω if the original coil is replaced (on the same nylon form) by un-tinned 1/8" diameter copper tubing with a wall thickness much greater than the skin depth. The result of the new coil is shown in Figures 7A, B. The top trace in Figure 7A is the diode voltage and the bottom trace is the Faraday Cup current. Figure 7B is the diode current. All conditions were identical, except for the coil change, to those in Figure 4C, D. The sensitivity was doubled in Figure 7B as compared to Figure 4D. By comparing the results of Figures 4C, D to 7A, B it is clear that the skin effect is not responsible for the reduction of the ripple.

To show that the nylon coil form did not provide attenuation by dielectric loss, the new coil was removed from the nylon form. Figure 8A, B shows the results. Again, the top trace in 8A is the diode voltage and the bottom the Faraday Cup current. Figure 8B is the diode current. Comparing Figures 8A, B to 7A, B, there is only a slight increase in the diode current ripple. Thus it can be concluded that the dielectric loss does not play a significant role in the ripple removal. It might also be argued that the liquid freon used in the high voltage tank could provide attentuation through dielectric loss. However, the surface area of the aluminum rod used to obtain the results in Figure 2A was larger than the surface area of the wire used in Figures 2B and C. Thus, the dielectric loss of the liquid freon is not an important factor in the attenuation mechanism of the ripple signal.

Overshoot From a Long Pulse

Figure 9 shows the reduction of overshoot in the diode voltage when the cathode is changed from a solid graphite disc to a hemispherical graphite brush (Fig. 10). The top trace in A is the Faraday Cup current and the bottom is the diode current. B is the diode voltage. A and B are produced using a flat graphite cathode. C is the diode current. The top trace in D is the diode voltage and the bottom trace is the Faraday Cup current. C and D are produced when a hemispherical brush cathode is used (Fig. 10). An initial overshoot is quite evident in B but is completely removed in the voltage trace in D.

The idea in using the graphite brush cathode was to increase the electric field at the cathode surface. The local electric field is enhanced at the point of emission since the charge density is much higher at an edge or point than over a large surface.

Beam Propagation

All previous work shown so far did not have an electron beam propagating over a significant distance. For the beam propagation study a foilless diode

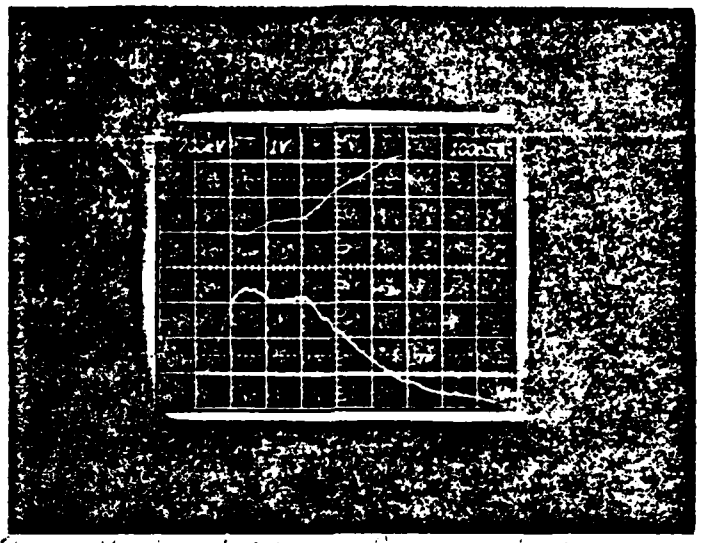

A

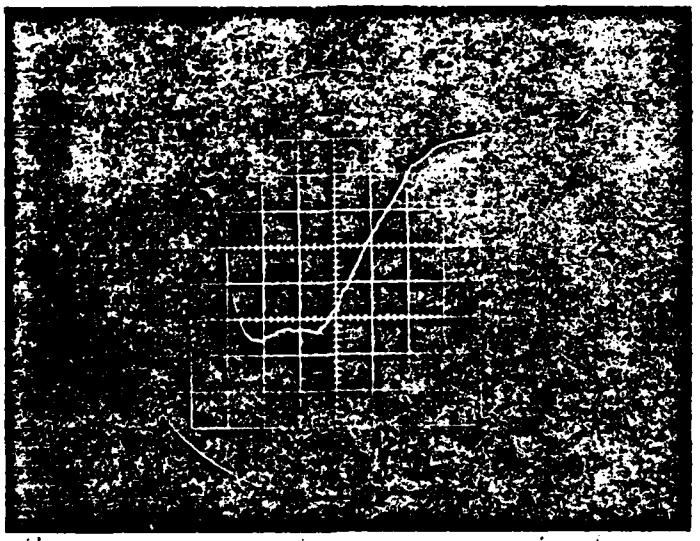

B

Figure 7

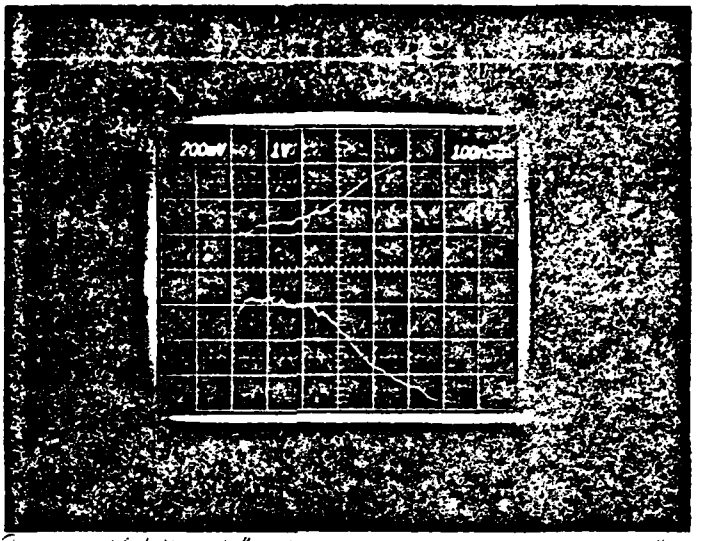

A

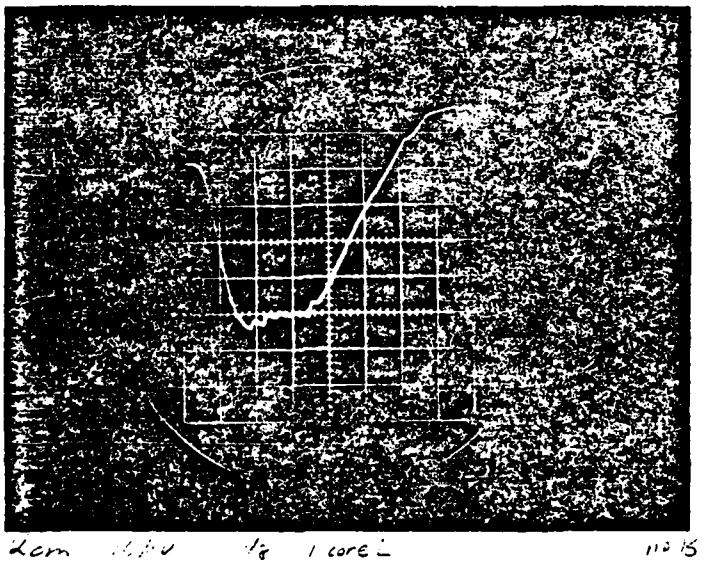

B

Figure 8

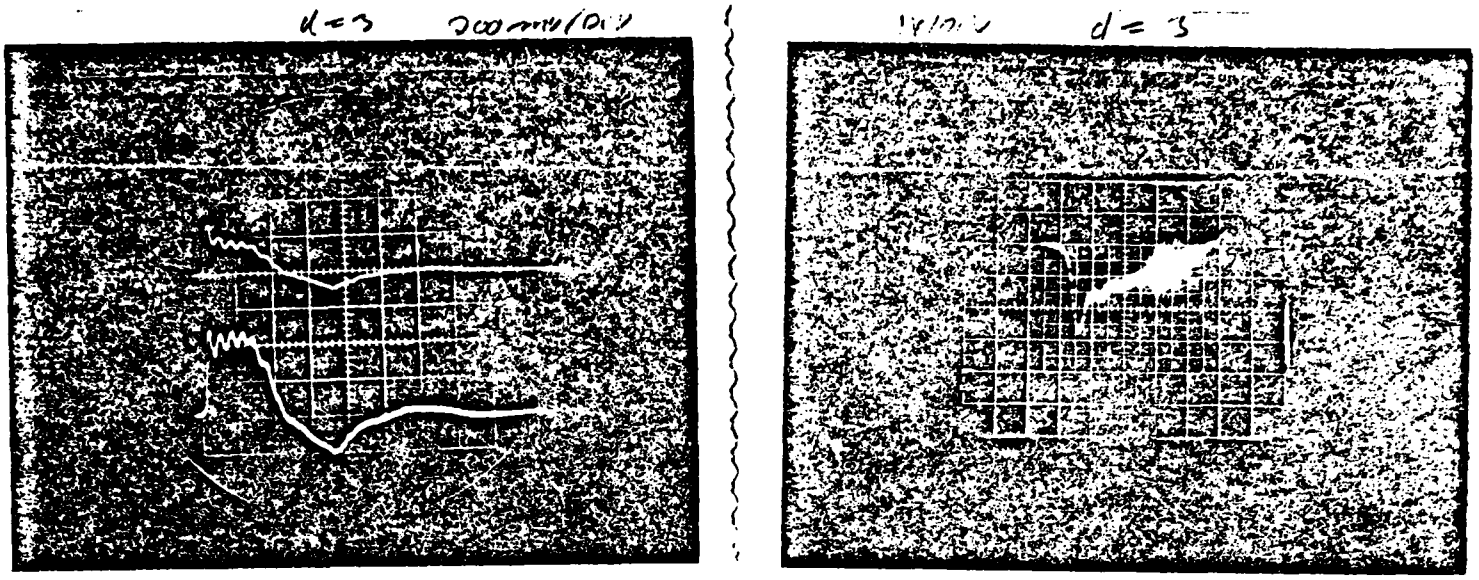

A B

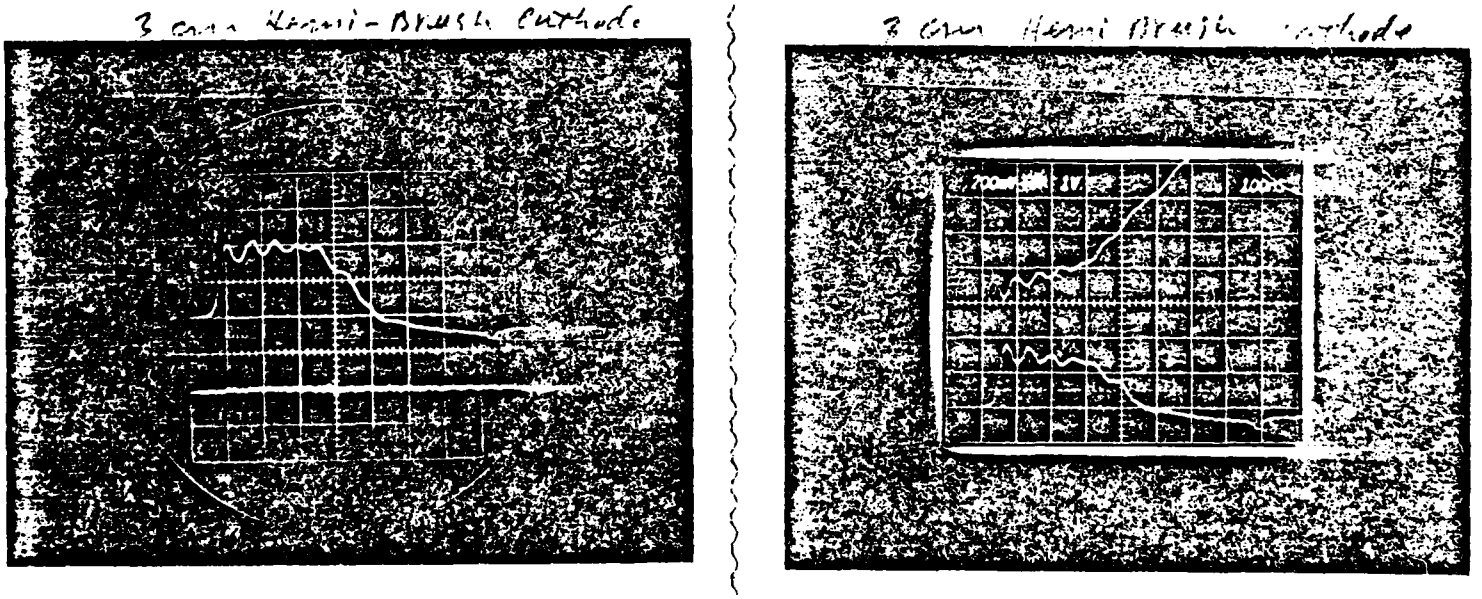

C D

Figure 9

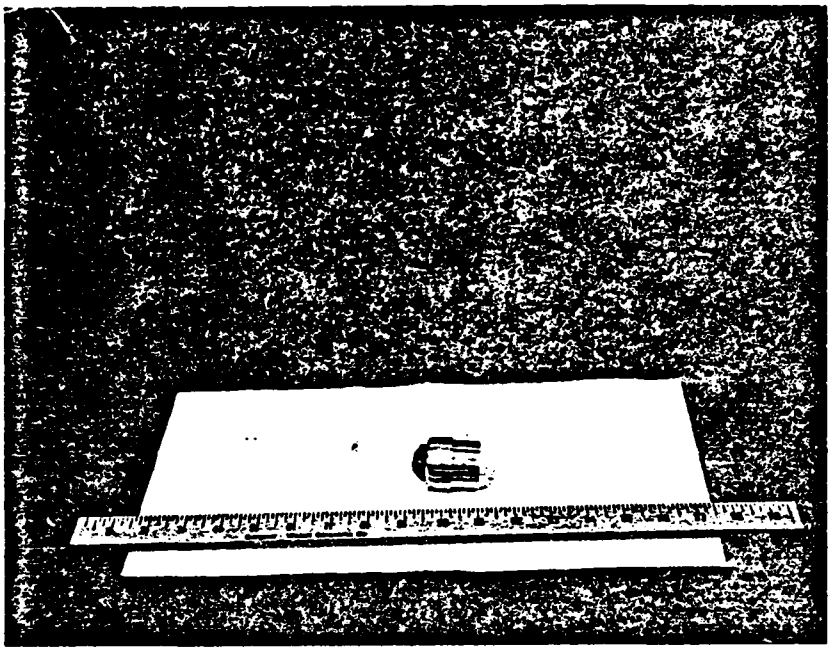

Figure 10

has been selected. A conical anode and cathode were initially tried (Fig. 1). Fig. 12A shows a frontal view of the graphite anode and Figure 12B shows the side view. Figure 13 shows the tapered cathode stock and the tapered graphite cathode tip. The cathode tip is partially unscrewed from the cathode stock. This tapered diode arrangement was designed to minimize the electric field stress on the cathode stock but to maximize the stress at the cathode tip. The idea was that the overstressed cathode would not have a "turn on" problem, as previously presented, and consequently would not have an overshoot in the diode voltage. However, overshoot did occur as shown in Fig. 11. The top trace in 11A is the diode voltage with a factor of two in overshoot and the bottom trace is the diode current.

The top trace in Figure 11B is the transmitted current. It too, has an overshoot which occurs because the transmitted beam current is close to the space charge limit current.[6-9] The Faraday Cup was located about 13 cm from the back of the graphite anode. The bottom trace in Figure 11B is the magnetic field current, which corresponds to a magnetic field strength of about 7.8 kG.

In order to eliminate the overshoot problem the tapered graphite cathode tip was replaced with a graphite brush (Fig. 15). Figure 14 shows the results from the graphite brush. The top trace in Fig. 14A is the diode voltage with the overshoot completely eliminated, and the bottom trace the diode current. Figure 14B is the corresponding transmitted current using a 15.5 kG magnetic field and having the Faraday Cup located 129 cm from the back of the anode. A relatively clean transmitted current is obtained, except for a droop in the current. This droop is of course related to the droop in the diode voltage, since the transmitted current is close to the space charge limit current.

Figure 16 is a plot of the peak transmitted beam current as a function of diode impedance at different magnet field strengths. It is clear that the

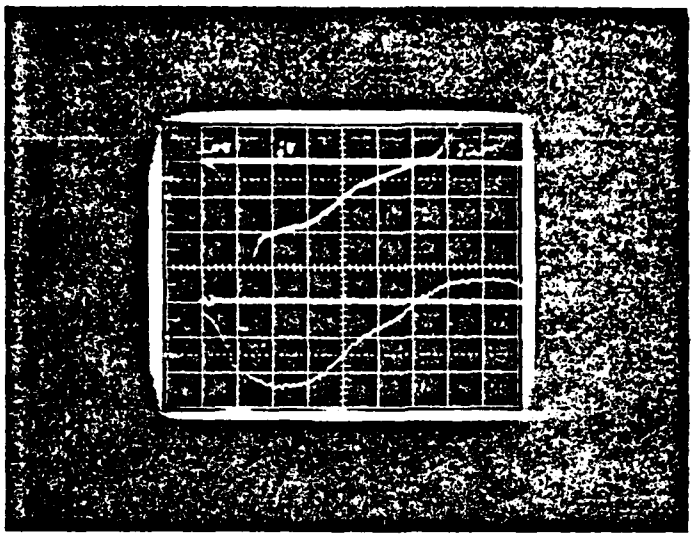

A

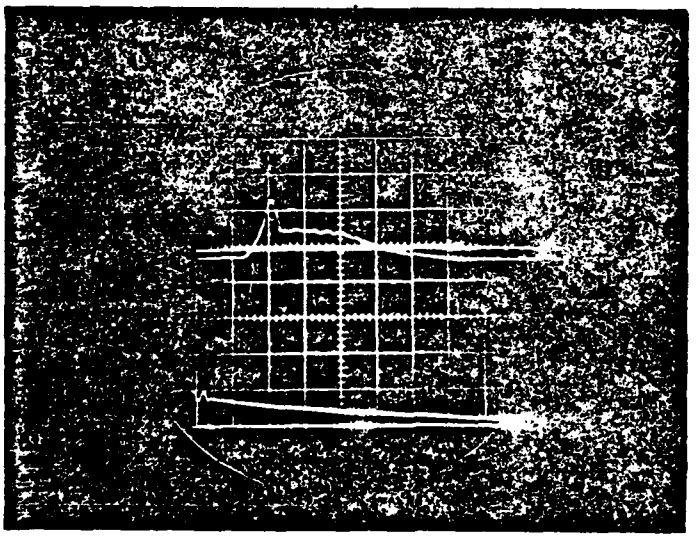

B

Figure 11

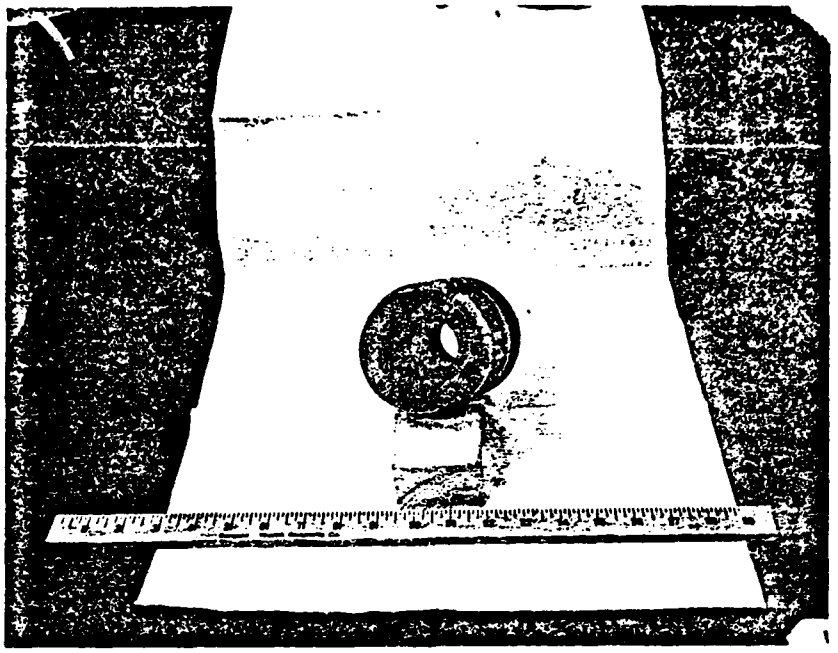

A

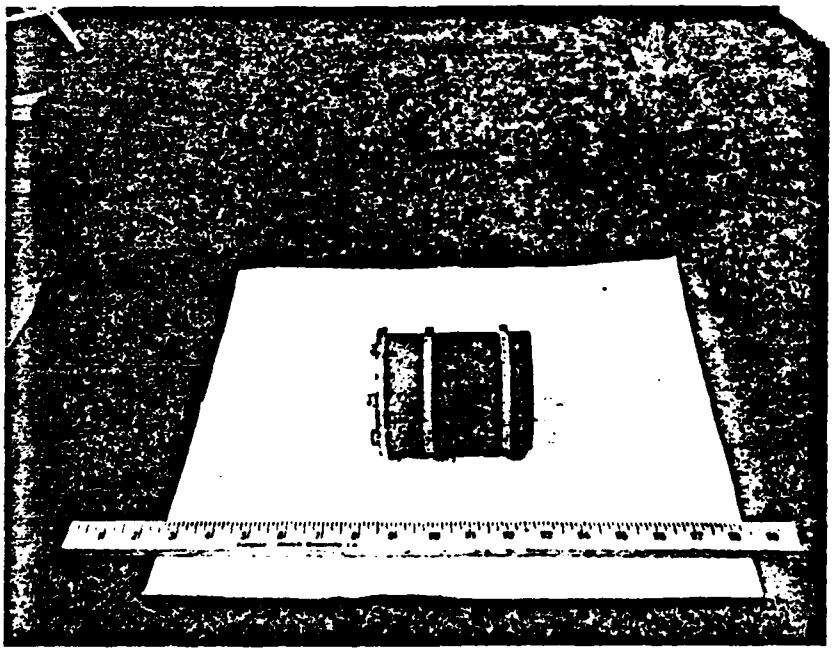

B

Figure 12

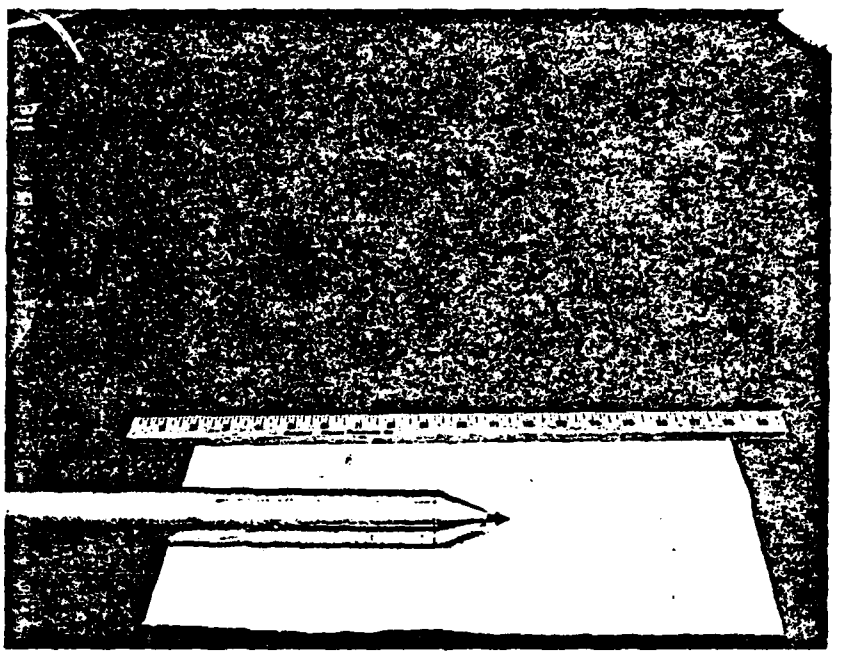

Figure 13

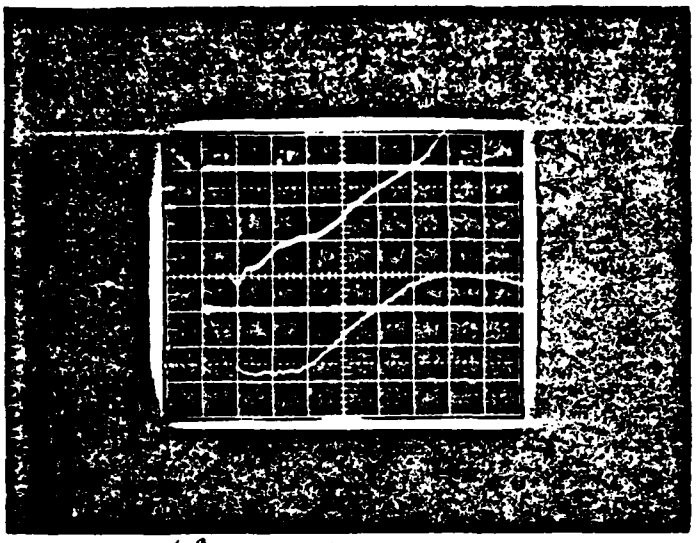

A

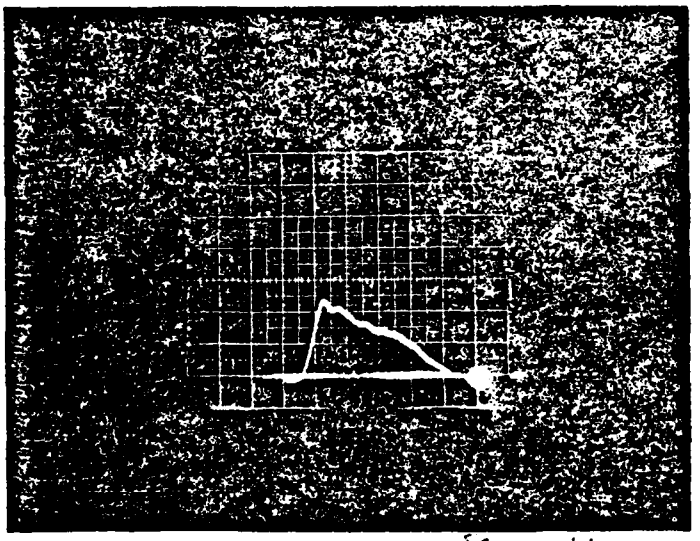

B

Figure 14

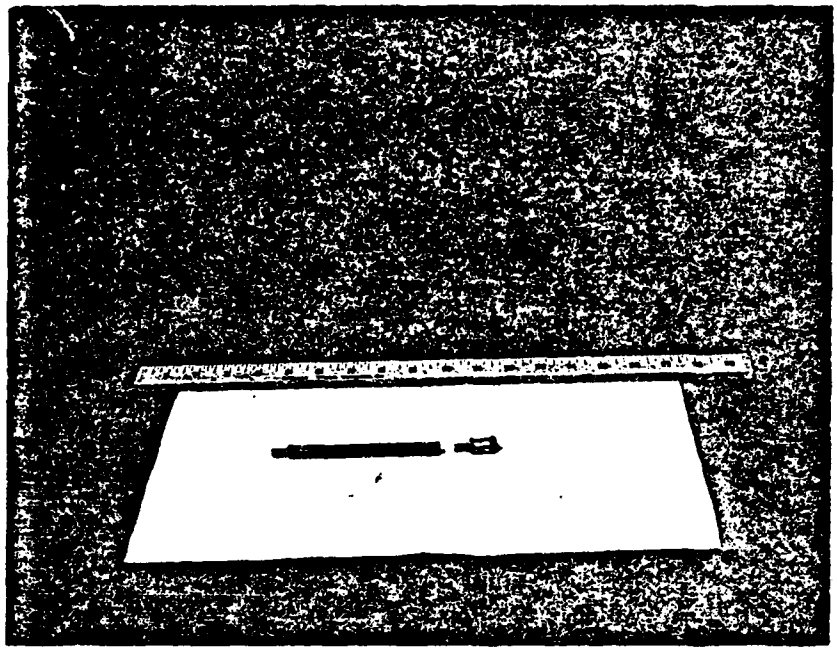

Figure 15

transmitted current reaches a maximum as the diode impedance becomes equal to the pulse line impedance (300Ω). This result would of course be expected. Since when the diode impedance is lower than the line impedance a lower diode voltage will reduce the limit current. At a diode impedance greater than the line impedance the high voltage gives a high limit current but the diode current is not available. The point of this exercise was to find a diode that could match to the line impedance and still produce a high quality beam.

In an attempt to get higher propagated currents another cathode was tried. This time a long graphite brush (Fig. 18) was used. The graphite brush was made from graphite string and constructed like a bottle brush. A plot of the transmitted current versus diode impedance at different magnetic field strengths is shown in Fig. 17. In this case slightly higher currents were transmitted, however the beam quality was reduced. An overshoot reappeared in the diode voltage.

4. . Summary and Conclusions

During the contractual period it became evident that additions to the proposal were necessary. One addition was now to produce a high quality electron beam. Thus, the results below reflect this change to the proposal.

A long pulse (300 ns FWHM) ripple free electron beam has successfully been propagated near its space charge limit current over a distance of 1.3 m in an axial magnetic field of up to 21 kG. Diode voltage and current ripple is known to be a property of discrete pulse lines. This ripple has been removed by a high frequency rejection technique. In this technique an inductor is used as a high impedance line to the high frequency components of the wave form. Diode voltage overshoot has also been removed. This effect occurs when the cathode electric field is too low for field emission currents to rapidly "turn on."

The overshoot was removed by using a locally spatial electric field cathode. A cathode constructed of graphite fibers provided the high stress field by utilizing the edge enhancement effect.

Droop in the diode voltage and transmitted beam was mentioned. Droop results when the cathode and anode plasmas collapse together. In going from the solid anode to the magnetically insulated foilless diode it would be expected that the anode plasma would be eliminated and thus a reduction in the voltage droop should appear. However, the results show no change in voltage droop, thus only the cathode plasma contributes significantly to the voltage droop. To remove the voltage droop the cathode plasma would have to be eliminated. But the formation of a cathode plasma is a necessity for the cold cathode mechanism of producing electrons. Thus, it can be concluded that the only way to get a higher quality (flat top) long pulse beam is by using a thermionic cathode.

An intense ion injector study has been done by computer simulation. One major problem in the reflexing beam mechanism has been partially solved. Previously, the acceleration process was shown to be phase unstable. This instability imposed a saturation limit to the maximum ion energy. By doubling the length of the acceleration system the ion velocity has shown a 10% increase without any signs of saturating.

A set of water cooled coils have been designed to give the maximum field for the least input power or energy for D.C. or pulse application. The specific design was for a racetrack configuration. Fifty coils at 28 turns/coil with an 8" I.D. and 4" x 5¼" cross section spaced 4" apart will produce 5k6 at 4ha D.C. and 10kG with a 1MJ capacitor bank. The field is over a 12 m path length with a 2% field variation from coil to coil.

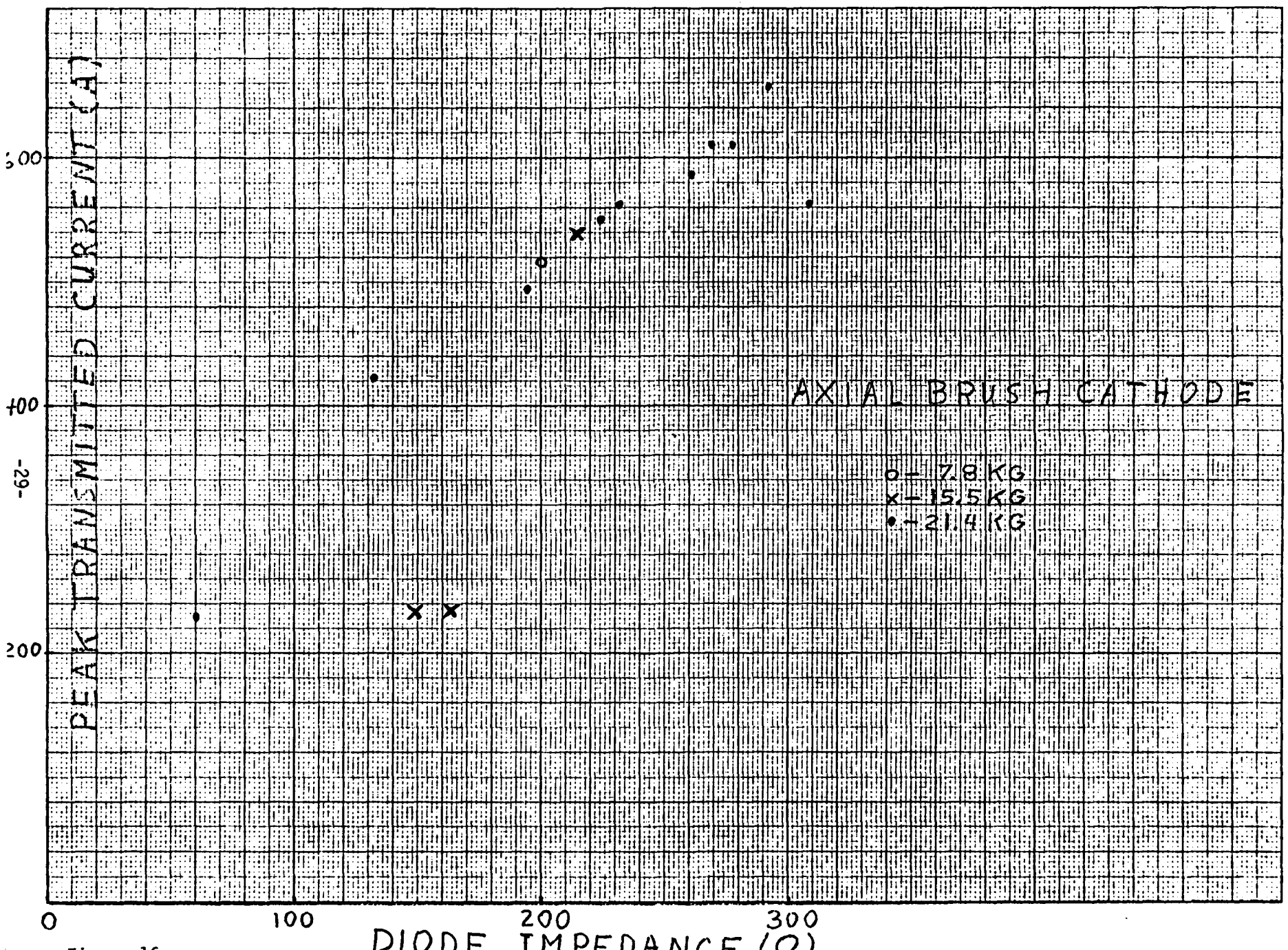

Figure 16

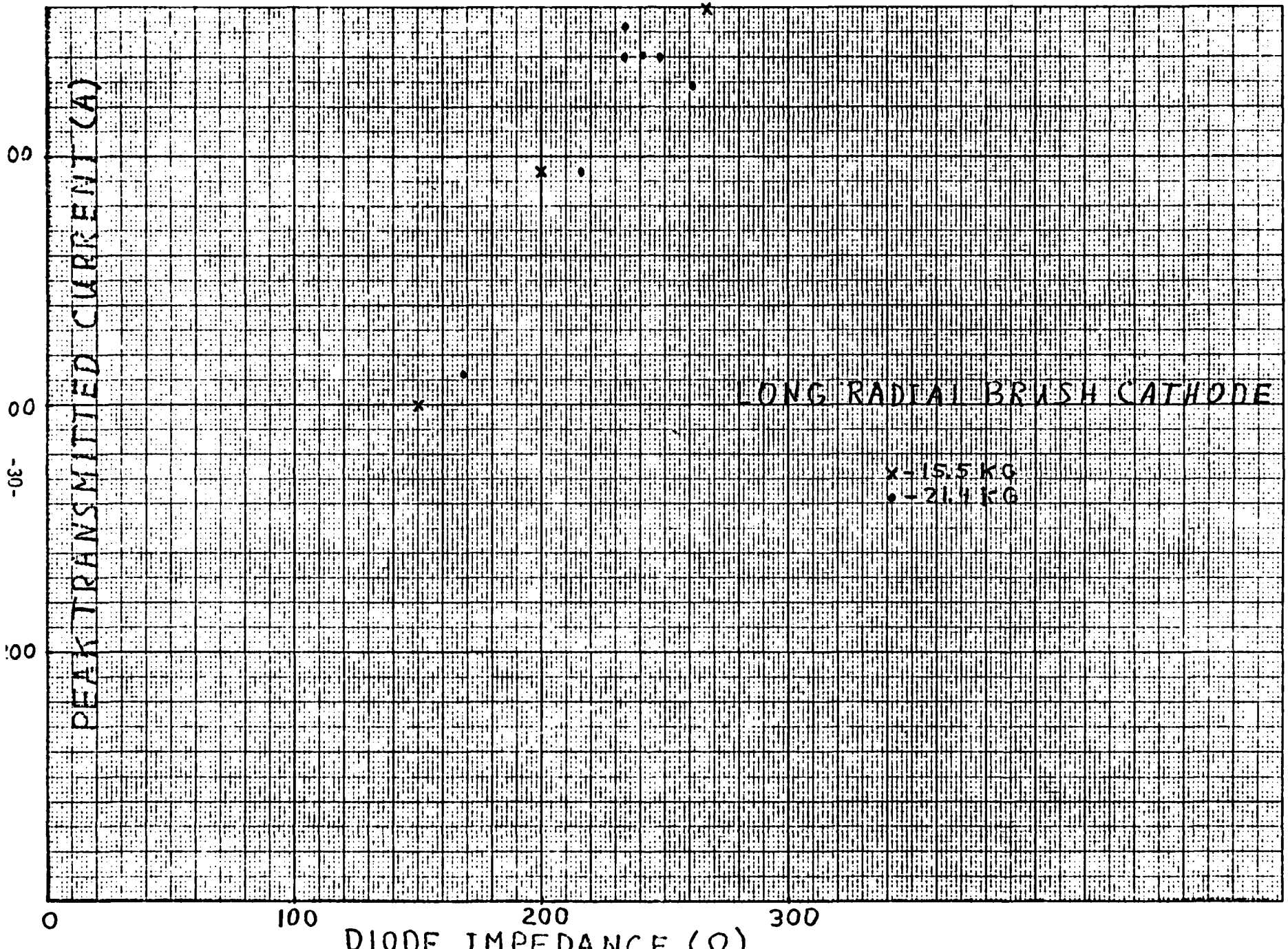

Figure 17

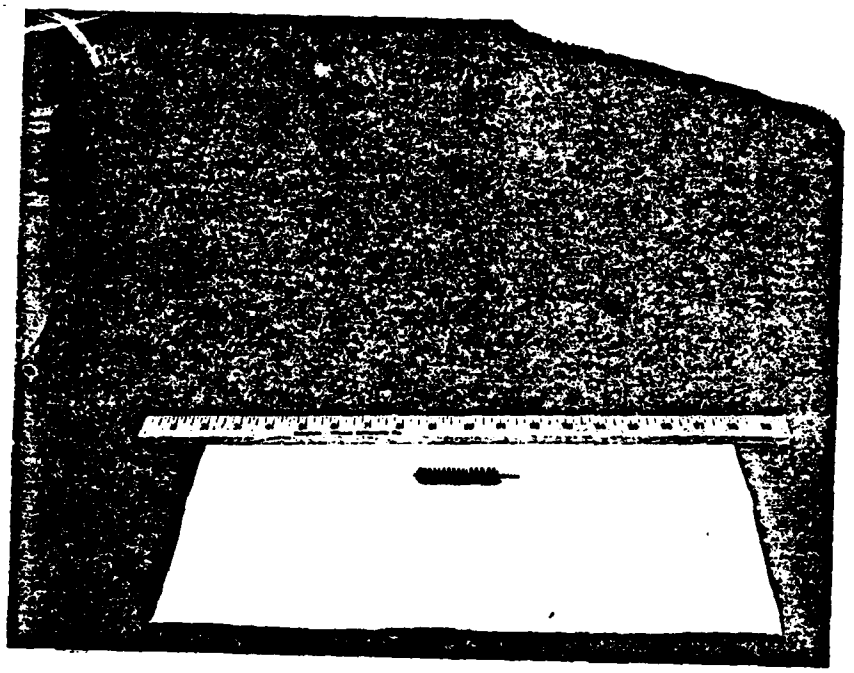

Figure 18

III. Intense Ion Injector Study

A. Introduction and Background

An intense ion injector should be able to accelerate a 1kA beam of ions from rest to about 50 MeV in order to be useful as a pre-accelerator for a space charge wave accelerator. A simulation study was carried out to examine the feasibility of a particular mechanism for ion acceleration.

One of the first explanations of ion acceleration from reflexing intense relativistic electron beam experiments was proposed by Ryutov and Stupakov. In their model, an intense electron beam is injected through a positively charged thin metal anode into a pre-formed plasma density gradient. The plasma density abruptly drops to zero in a short distance beyond the anode. This configuration forces the beam to turn around in its own space charge at the position of the virtual cathode. Thus, with the anode voltage being applied to the returning electrons, the beam is forced into an oscillatory or reflexing condition. In this model an infinite magnetic field is applied along the direction of beam propagation thus constraining the model to be one dimensional. Also, the beam does not have a bulk rotation ("slow mode") but can acquire Larmor rotation. Larmor rotation or electron thermalization is provided, in the optimal ion acceleration case, by elastic scattering of the beam as it passes through the anode foil.

Ion acceleration takes place by the ambi-polar diffusion mechanism. That is, the ions located at the plasma vacuum boundary are accelerated by the space charge electric field of the reflexing electrons which extend into the vacuum region. Ions are therefore accelerated in the direction of beam propagation. Since the ions move towards the virtual cathode and the virtual cathode cannot move without the ions, one might expect that the ions and virtual cathode move in a synchronous fashion. Thus, one would expect

the ions to acquire a high final energy. The ion energy would of course be bounded above by the ion to electron mass ratio times the initial electron energy. That is, when the ions reach the initial electron velocity.

B. Results

Starting parameters were selected to minimize run time and hence cost. The distance between the beam injection and absorption planes was 15 cm. The initial spatial extent at plasma from the injection plane was .5 cm. A beam density of 1.3×10^{10} cm^{-3} was typically used with a plasma density of 1×10^{12} cm^{-3}. A cyclotron frequency of about three times the plasma frequency was used. The beam velocity was .67 c with an electron thermal velocity of .1 c.

The electron and ion temperatures were initially equal and an ion to electron mass ratio of 20 was used.

At 60/wpe the ions have reached their maximum energy, which is about three times the electron energy. The acceleration process has become phase unstable. That is, the peak in the electric field amplitude is spatially out of synchronization with the ions of maximum energy. This result has been previously established by Mako and Tajima.[10] The point of repeating this result was as a check and to establish a baseline. Several attempts were made by these authors to break up the instability, however, nothing appeared to work.

When the problem was re-evaluated by S. Kainer and F. Mako a new approach was taken. It appeared that the acceleration processed saturated when the first electron reached the far absorption well. This implies a loss of momentum in the acceleration region. Thus, a simple solution would be to lengthen the system. So the spacing between the injection and absorption planes was doubled.

After doubling the system length, a 20% increase in the ion energy resulted. This increase is not dramatic and the explanation may not be correct, however, there were no signs of saturation during the run time of up to 60/wpe.

If this study were to continue the following action would be taken:

1) Simply run the code for a longer time to determine if and when saturation sets in again.

If saturation reappears then the system length would be extended again, until a relationship could be established between system length and saturation. With this new information a new direction could be established, if necessary.

2) Try increasing the beam to plasma density ratio. This increases the beam power and should speed up the acceleration process.

3) Put a ramp increase on the electron energy. This would be done in such a way as to keep the peak electric field in synchronization with the maximum ion energy.

4) To circumvent the cause and cure the symptom, plasma blobs could be turned on at the position of and time of the appearance of the phase instability. These plasma blobs serve to locally neutralize the virtual anode and allow it to relocate, such as to maintain synchronization.

IV. Toroidal Magnetic Field Design

A. Introduction

A new and novel electron accelerator concept has been proposed by C. W. Roberson of NRL. This accelerator has been named, the Racetrack Induction Accelerator (RIA). The RIA is compact and capable of producing high current high energy electron beams. Applications of such a beam might be for space charge wave accelerators, free electron lasers and directed energy research.

The idea is to continually apply an electric field to a circulating beam of electrons. This idea is not new and has been used in conjunction with low current electron beams (<1A). In order to have a high current beam (~1kA) something must be done to suppress the beam from expanding in its own space charge. Expansion of the beam is suppressed by using a toroidal magnetic field, which is new. Figure 19 is a drawing of the RIA, shown are the vacuum chamber and induction modules, which supply the electric field in the gaps. Figure 20 shows a top view of the RIA with just the magnetic coils necessary for producing a toroidal magnetic field. A table of the RIA magnetic field specifications is given in Section A, 1. Sections B, C, D present the design considerations given, in an effort to generate the desired magnetic field.

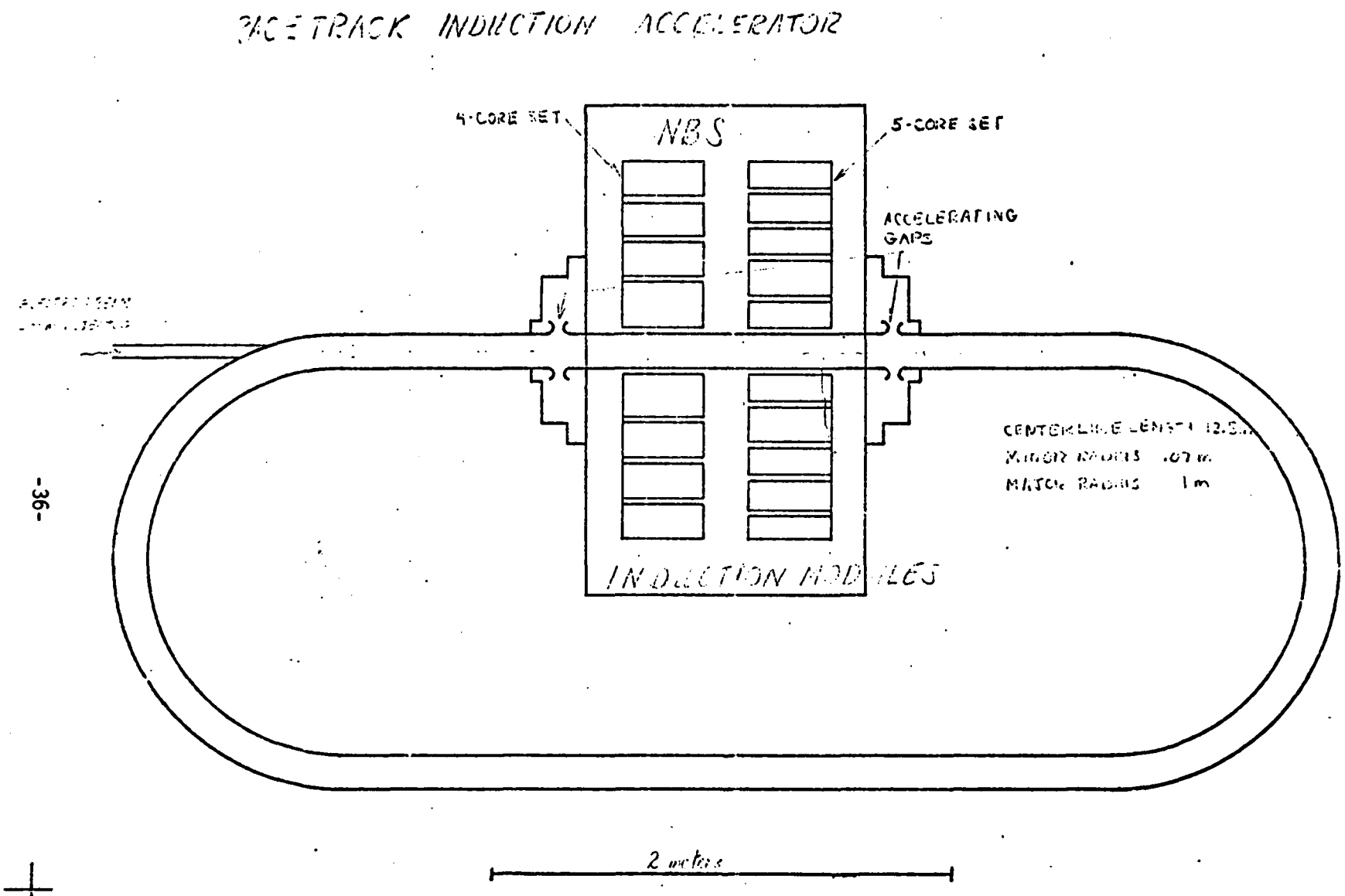
RACETRACK INDUCTION ACCELERATOR
4-CORE SET
NBS
5-CORE SET
ACCELERATING GAPS
INDUCTION MODULES
2 meters

Figure 19

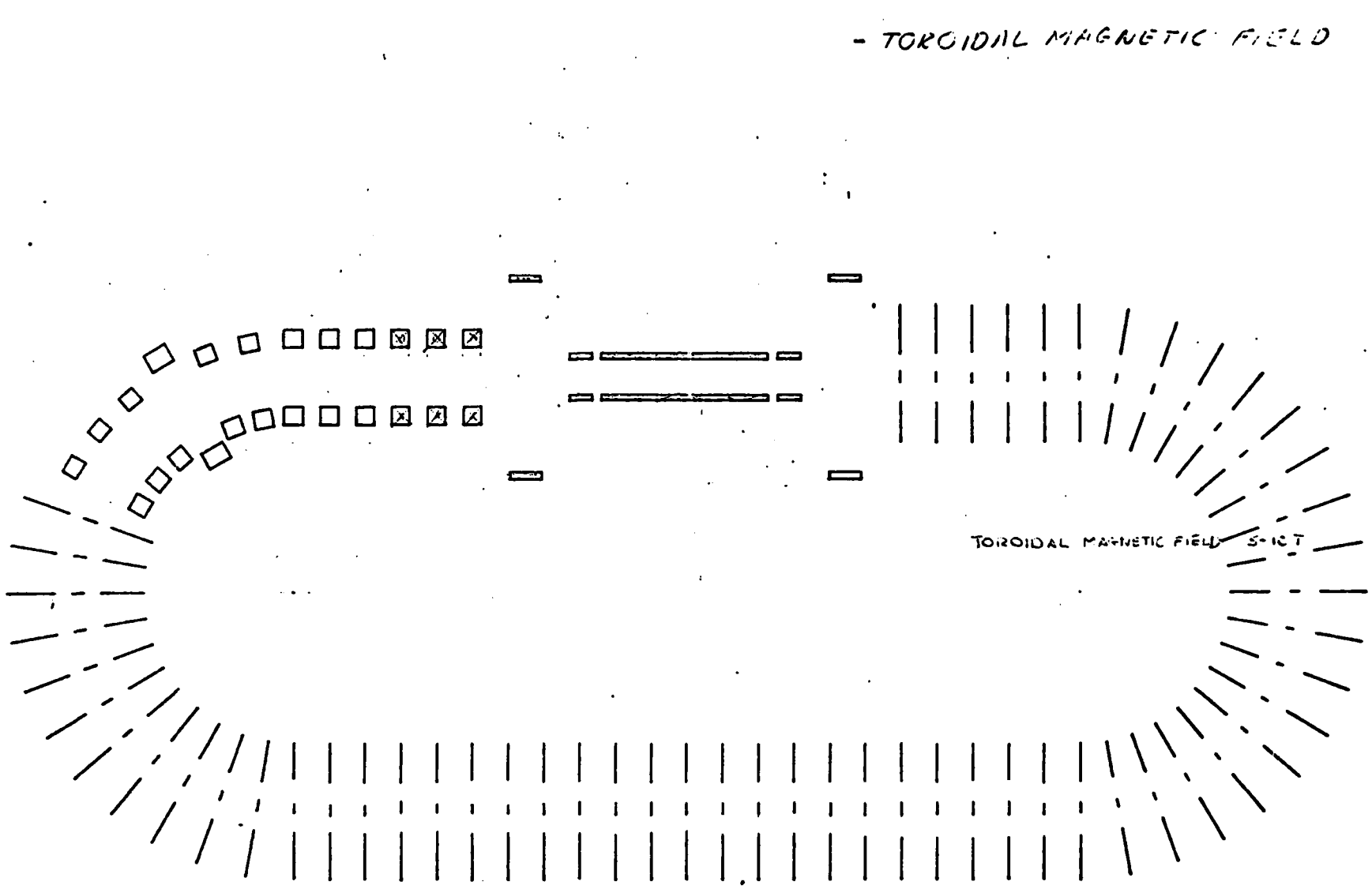

Figure 20

1. Racetrack Magnetic Field Coils, Specifications

a. Max. Field Strength: 5 kG D.C. at 4 kA (on axis of racetrack)
10 kG Pulse (Cap. discharge)

b. Spatial Length of Field: 12 m

c. Inside Diameter of Field: 20 cm

d. Coil Spacing (face to face): 10 cm

e. Field Uniformity: 1% Coil center to center on axis

f. Total Coil Resistance: 50 mΩ matched load to power supply

g. Water Flow Rate: <1200 Gal./min at 150 PSI

B. Electrical Design

1. Optimum Coil Cross Section

In this section the individual coils are designed for efficient production of both D.C. and pulsed magnetic fields. For D.C./pulse operation efficiency means that the coil cross section is selected to give the maximum field with a minimum in the power input/capacitor bank energy, respectively.

Efficiency is important in this particular application because of the conditions imposed on the problem. These conditions are the large magnetic field in a large volume.

Starting from the Biot-Savart law for a loop of wire of zero cross-section, the field is,

$$B_z(r=o,z) = \frac{\frac{1}{2}\mu_o I a^2}{\left[(z-z^1)^2 + a^2\right]^{3/2}} \quad . \text{ (MKS units)} \qquad (1)$$

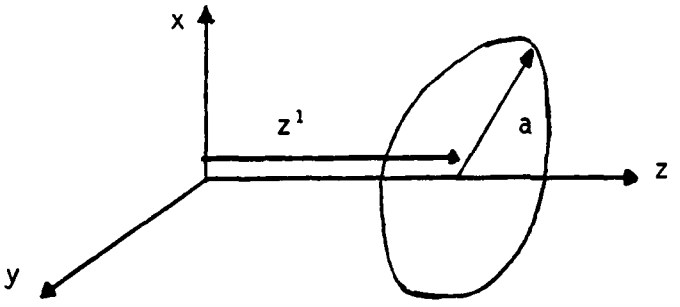

μ_o - permeability of free space

I - current (Amp)

Eq. (1) can be easily integrated for a finite cross section wire

$$B_z(r=o,z) = \frac{-\frac{1}{2}\mu_o I}{(a_2-a_1)(z_2-z_1)}\left[(z-z_2)\left| n\left(\frac{a_2 + \sqrt{a_2^2 + (z-z_2)^2}}{a_1 + \sqrt{a_1^2 + (z-z_2)^2}}\right)\right.\right. \qquad (2)$$

$$\left. - (z-z_1)\left| n\left(\frac{a_2 + \sqrt{a_2^2 + (z-z_1)^2}}{a_1 + \sqrt{a_1^2 + (z-z^1)^2}}\right)\right.\right]$$

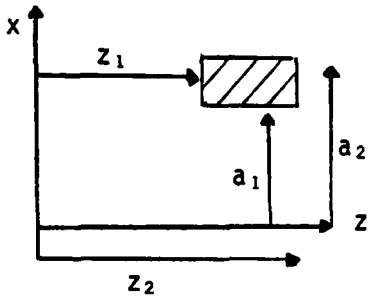

$$\alpha = \frac{a_2}{a_1}$$

$$\beta = \frac{z_2 - z_1}{z a_1}$$

Now if the field is solved for in terms of the power then,

$$\beta = G(\alpha,\beta)\,\frac{5}{2\pi}\,\mu_o\left(\frac{P}{\rho a_1}\right)^{\frac{1}{2}} \qquad (3)$$

P - power (watts)

ρ - resistivity (Ω-m)

where

$$G(\alpha,\beta) = \frac{1}{5}\left(\frac{2\pi\beta}{\alpha^2-1}\right)^{\frac{1}{2}} \left| n\left[\frac{\alpha + (\alpha^2 + \beta^2)^{\frac{1}{2}}}{1 + (1 + \beta^2)^{\frac{1}{2}}}\right]\right. \qquad (4)$$

This geometric factor is plotted (Fig. 21) and has a maximum at $\alpha = 3$, $\beta = 2$. A coil with $\alpha = 3$, $\beta - 2$ will produce the most field for the least power (D.C.). However, the coils would be very poor for pulsed application, since the radial volume is large. Since the geometric factor is broad banded a compromise can be made for both pulsed and D.C. application. If an 80% efficient D.C. design is picked then G =.143 and if we select a relatively small coil $\beta = .65$, $\alpha = 2$ . .

or for an 8" I.D. coil

$a_2 - a_1 = 4"$

$z_2 - z_1 = 5.2"$

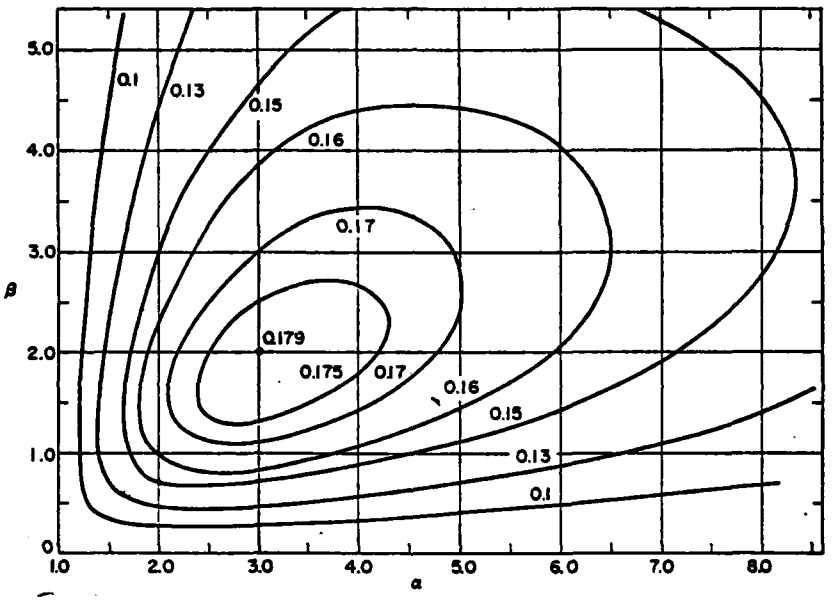
0.1
0.13
0.15
0.16
0.17
0.179
0.175
0.17
0.16
0.15
0.13
0.1
5.0
4.0
3.0
2.0
1.0
0
β
1.0
2.0
3.0
4.0
5.0
6.0
7.0
8.0
α

Figure 21

This coil size will make the pulse field about 67% efficient, since

$$B_z \propto \frac{1}{D_m} \tag{5}$$

where D_m is the mean diameter of a solenoid.

The damping factor is neglected in the pulse calculation, it will however not be important but is checked in Section 5.

2. Total Number of Turns

By integrating around the racetrack axis the field is

$$B_z = \frac{\mu_o NI}{\ell} \quad \text{(MKS)} \qquad \begin{array}{l} N \text{ - total no. of turns} \\ \ell \text{ - total path length} \end{array} \tag{6}$$

for ℓ = 12 m I = 4 kA $\mu_o = 4\pi \times 10^{-7}$ B_z = 5 kG

N = 1200

Since we have neglected a loss of field due to the spacing between coils, it will be assumed that only 80% of the desired field can be produced. To compensate for this field loss 25% more windings will be added. Thus

N = 1500 turns

For the previous coil size and a spacing of 10 cm, 50 coils are needed with 30 turns per coil.

3. Winding for Field Purity

The idea here is to cancel the axial current with the windings. This is shown below.

A. No cancellation. Produces B_θ field impurity.

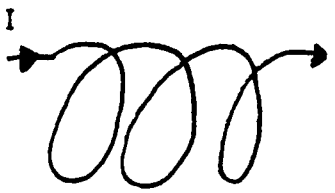

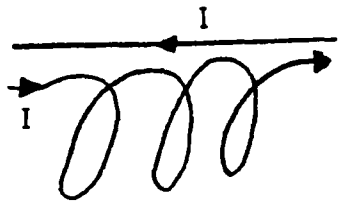

B. Cancellation by return wire.

Partial reduction of B_Θ field.

C. Cancellation by return winding.

Complete removal of B_Θ field.

4. Selection of Wire Size

The coil resistance is given by

$$R = \frac{\rho n \pi D_m}{A} \qquad (7)$$

ρ - resistivity (Ω - m)

n - no. of turns per coil

D_m - mean coil diameter

A - wire cross section

For 50 coils

$R = 1\ m\Omega$ and $n = 30$ $D_m = 30$ cm $\rho = 1.7 \times 10^{-8}\ \Omega$-m

$A = 4.85\ cm^2$ ($\simeq \frac{3}{4}" \times 1"$)

Rectangular wire that is 1/2" x 3/4" is commercially available. Thus a parallel winding made of 2 wires 1/2" x 3/4" could be used. One way to do this is shown below.

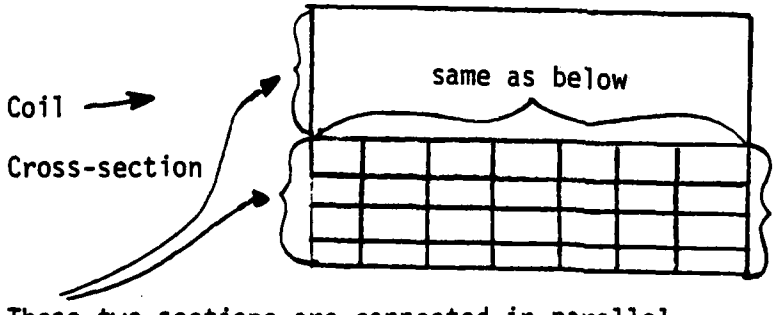

28 turns series wound with cancellation windings

These two sections are connected in parallel

5. Capacitor Bank Size

With 100% transfer of capacitor bank energy to magnetic energy the field is given by

$$B_z = \sqrt{\frac{2\mu_o \varepsilon_b}{\ell\left(\frac{\pi D_m^2}{4}\right)}} \quad \text{(MKS)} \qquad \varepsilon_b \text{ - bank energy (joules)} \tag{8}$$

for B_z = 10 kG, ℓ = 12 m D_m = 30 cm $\varepsilon_b \simeq 1$ MJ Required Cap. at 10 kV

$C = 20$ mF

Now checking the efficiency factor or attenuation factor k(d). The maximum current in an under damped discharge is

$$I_{max} = k(d)\, V_o \sqrt{\frac{C}{L}} \tag{9}$$

V_o - charge voltage (V)

C - capacitance of bank (F)

L - coil inductance (H)

$$k(d) = \exp\left[-\left(\frac{d}{1-d}\right)^{\frac{1}{2}} \tan^{-1}\left(\frac{1-d}{d}\right)^{\frac{1}{2}}\right] \tag{10}$$

$$d = \left(\frac{R}{2\sqrt{\frac{L}{C}}}\right)^2 \tag{11}$$

$$L \simeq \frac{\mu_o N^2 \frac{\pi}{4} D_m^2}{\ell} \simeq 17\text{mH} \tag{12}$$

$d = 7 \times 10^{-4}$ (see Figure 22 for a plot of k(d))

therefore, $k \simeq .97$

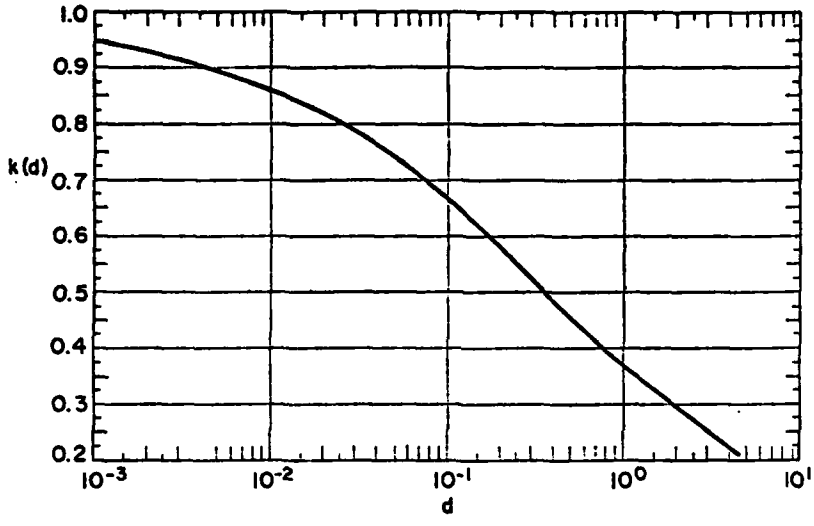

Figure 22

C. Cooling and Hydraulic Considerations

1. Volume Rate of Coolant

The flow rate is determined by the power and the coolant.

$$\dot{V}\left(\frac{cm^3}{sec}\right) = \frac{P\ (watts)}{\rho\left(\frac{gm}{cm^3}\right)\ Cp\left(\frac{J}{gm\ C}\right)\ \Delta T\ (^{\circ}C)} \qquad (13)$$

For water $Cp = 4.18\ \frac{J}{gm\ C}$ at 20 C & 1 Atm.

$$\rho = .988\ \frac{gm}{cm^3} \text{ at } 50\,^{\circ}C$$

and $\Delta T = 25\ ^{\circ}C$

then

$$\frac{\dot{V}}{P} \approx \frac{150\ Gal/min}{MW}$$

For the power supply being used P = .8 MW

thus

$$\underline{\dot{V} = 120\ Gal/min}$$

2. Pressure Drop in Coils

As it turns out, for the necessary flow rate to cool the coils the flow is turbulent and thus makes calculating the pressure drop more difficult.

The pressure drop is given by

$$\Delta P(PSI) = 4.375 \times 10^{-2}\ f\ \frac{L\ (ft)}{D^5(ft)}\ V^2\left(\frac{ft^3}{sec}\right)$$

L - is the tube length

D - tube diameter

V - volume flow rate

f - friction factor

The friction factor depends on the tube roughness and the fluid velocity. A set of curves are provided for determining both the roughness factor (e in Fig. 23) and thus the friction factor (Fig. 24)

The hole diameter that is available for the 1/2" x 3/4" wire is 1/4". This diameter increases the resistance by 10% but is not too small for particulate matter to be trapped in.

Assuming drawn tubing (Fig. 23) then

$$\frac{D}{e} = 5 \times 10^4$$

from a flow rate of $\frac{1.2 \text{ Gal}}{\text{min}} \left(2.68 \times 10^{-3} \frac{\text{ft}^3}{\text{sec}}\right)$

for each coil with <u>two</u> passages (upper and lower half of coil in parallel) the velocity is

$$v = \frac{4 \dot{V}}{\pi D^2} \approx \frac{7.86 \text{ ft}}{\text{sec}} \approx \frac{240 \text{ cm}}{\text{sec}}$$

The Reynolds number is then

$$Re = \frac{\rho_m v D}{\mu} = 3.4 \times 10^4 \quad \left(\mu = .3 \times 10^{-3} \frac{\text{lbm}}{\text{ft-sec}} \text{ at } 150^\circ\text{F}\right)$$

μ - viscosity

ρ_m - mass density

From Fig. 22 $f \simeq .006$

The tube length $L = N \pi D_m \simeq 44$ ft (N = number of turns per coil = 28)

<u>ΔP (PSI) = 21 PSI</u>

3. <u>Efficient Heat Transfer</u>

It is important to know that the heat in the wire can efficiently be transferred to the fluid.

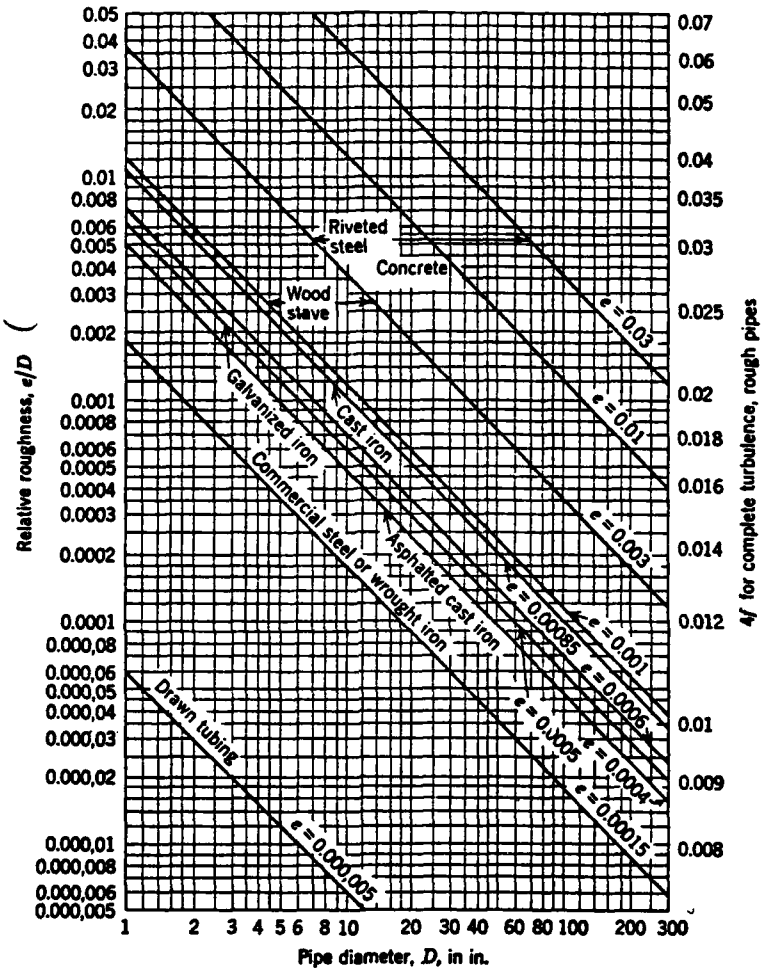
Relative roughness, e/D
0.05
0.04
0.03
0.02
0.01
0.008
0.006
0.005
0.004
0.003
0.002
0.001
0.0008
0.0006
0.0005
0.0004
0.0003
0.0002
0.0001
0.000,08
0.000,06
0.000,05
0.000,04
0.000,03
0.000,02
0.000,01
0.000,008
0.000,006
0.000,005
Riveted steel
Concrete
Wood stave
Galvanized iron
Cast iron
Commercial steel or wrought iron
Asphalted cast iron
Drawn tubing
e = 0.03
e = 0.01
e = 0.003
e = 0.001
e = 0.0006
e = 0.0004
e = 0.00085
e = 0.0005
e = 0.00015
e = 0.000,005
1 2 3 4 5 6 8 10 20 30 40 60 80 100 200 300
Pipe diameter, D, in in.
4f for complete turbulence, rough pipes
0.07
0.06
0.05
0.04
0.035
0.03
0.025
0.02
0.018
0.016
0.014
0.012
0.01
0.009
0.008

Figure 23

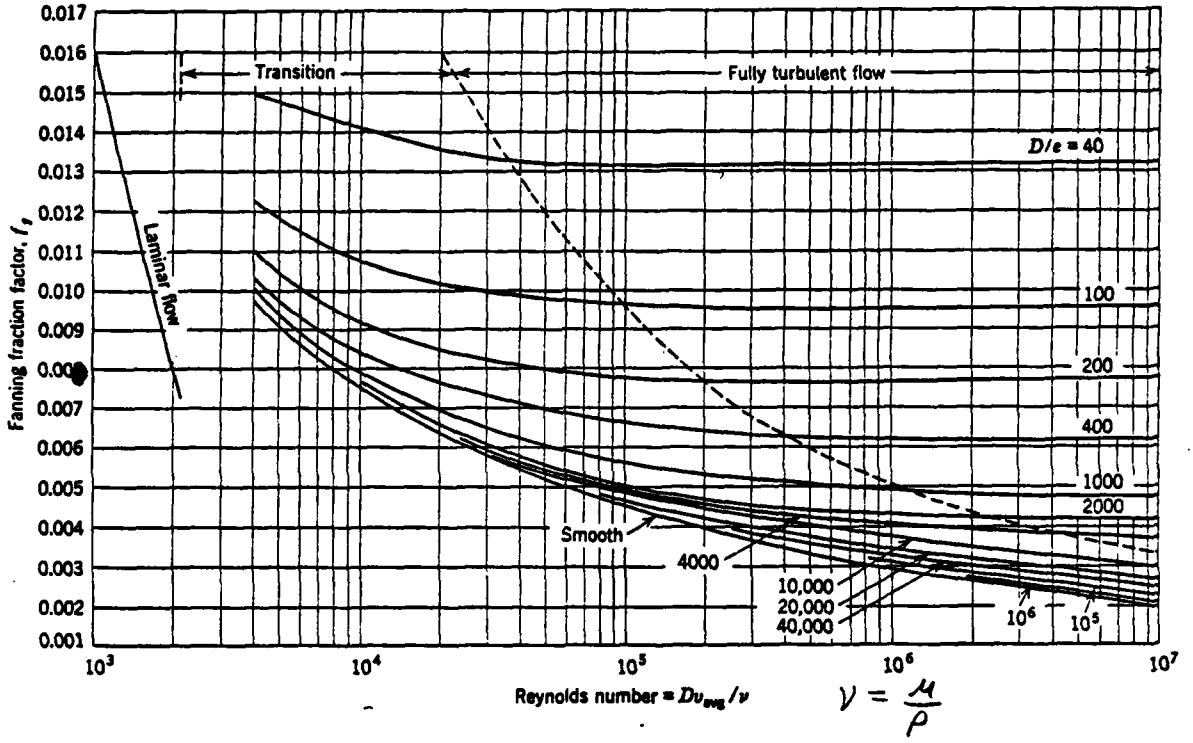
Transition
Fully turbulent flow
Laminar flow
Smooth
D/e = 40
100
200
400
1000
2000
4000
10,000
20,000
40,000
10^6
10^5
Fanning friction factor, f_F
Reynolds number = Dv_avg/ν
ν = μ/ρ

Figure 24

The heat convection equation is given by

$$T_w - T_b = \frac{Q\left(\frac{\text{watts}}{\text{cm}^2}\right)}{h\left(\frac{\text{watts}}{\text{cm}^2\,^\circ\text{C}}\right)} \qquad (15)$$

where; Q = heat flux over the surface in contact with the fluid

T_b = fluid temperature (°C)

T_w = wall temperature (°C)

h is the convective heat transfer coefficient.

For turbulent flow h is

$$h = 9 \times 10^{-3} \left(1 + 1.5 \times 10^{-2}\, T_b\right) \frac{v^{.8}}{D^{.2}}$$

for T_b = 50 C $\quad v = \frac{240 \text{ cm}}{\text{sec}} \quad D = .6$ cm $\quad h = 156$

for $Q \cong \frac{3w}{\text{cm}^2}$ then

$$T_w - T_b \cong 2 \times 10^{-2}$$ (thus the heat is being carried away efficiently)

4. Thermal Gradients

The thermal gradient in the conductor itself is

$$\Delta T = \frac{Wd^2}{2k} \qquad (16)$$

d - distance to cooling surface

W - power density $(\frac{\text{watts}}{\text{cm}^3})$

k - thermal conductivity of copper $(4.8 \frac{\text{watts}}{^\circ\text{C/cm}})$

for $W = 2.5 \frac{\text{watts}}{\text{cm}^3}$, d = 1 cm

$\underline{\Delta T = .26\,^\circ\text{C}}$, hence there are no hot spots in the conductor.

The thermal gradient for the insulation around the conducting surface is

$$\Delta T = \frac{Q\,\Delta x}{k_I}\,, \quad \text{where } Q \text{ - heat flux}\left(\frac{\text{watts}}{\text{cm}^2}\right) \tag{17}$$

Δx - insulation thickness (cm)

k_I - insulation conductivity $\left(\frac{W}{\text{cm}\,^\circ\text{C}}\right)$

for mica $\Delta x = .025$ cm

$$Q = \frac{3w}{\text{cm}^2}$$

$$k_b = 4.8 \times 10^{-3}$$

$\underline{\Delta T \quad 16\,^\circ\text{C}}$, therefore not much heat can be carried away through the insulator.

D. Field Analysis

1. Field Uniformity

Equation (2) has been written into a calculator program. This program can evaluate the field on axis for an arbitrary distribution of coils which are cylindrically symmetric.

The program shows a 2% variation of the field for a set of coils similar to the ones presented.

V. References

1. N. Rostoker and M. Reiser, Collective Methods of Acceleration, Harwood 1979.
2. R. Hendrickson, Editor, IEEE Trans. Nucl. Sci., Particle Accel. Conf. NS-26 No. 3 Part 2, p. 4155, San Francisco (1979).
3. P. Sprangle, A. T. Drobot and W. M. Manheimer, Phys. Rev. Letters. 36, 1180 (1976).
4. N. Rostoker, in Proceedings of the Seventh International Conference on High Energy Accelerators, Pub., Publishing House of Academy of Sciences of Armenia, Yerevan, SSR, 2, 509 (1970).
5. R. J. Briggs, Phys. Fluids 19, 1257 (1970).
6. L. E. Thode, B. B. Godfrey, and W. R. Shanahan, Phys. Fluids 22(4) (1979).
7. L. S. Bogdankevich and A. A. Rukhadze, Soviet Physics Uspekhi 14(2) (1971)
8. R. B. Miller and D. C. Straw, J. of Appl. Phys. 48(3) (1977).
9. M. L. Sloan and J. R. Thompson, Phys. Fluids (1977).
10. F. Mako, Thesis "Collective Ion Acceleration Controlled by a Gas Gradient", 1979. University of California at Irvine, California.

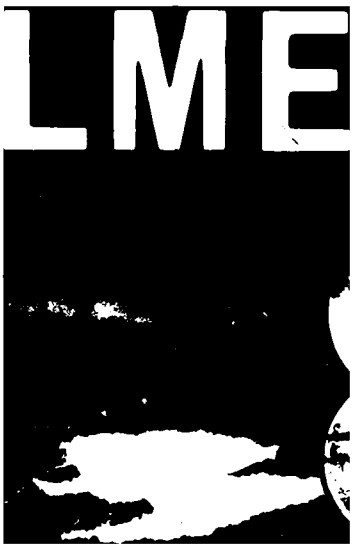
LME